Glass Alteration and Sediment Cementation Shikoku Basin, Offshore Japan

Russell J. White

Advisor: Dr. Glenn A. Spinelli

July 09

Department of Earth and Environmental Science
New Mexico Institute of Mining and Technology

ABSTRACT

Chemical analyses of volcanic glass from Shikoku Basin (offshore southern Japan) provide insight into volcanic source terrains, sediment dispersal mechanisms, and glass alteration and cementation processes that are not evident from basic sedimentologic and petrographic techniques. Previous studies at Ocean Drilling Program (ODP) Sites 1173, 1174 and 1177 in Shikoku Basin suggest that a minor amount of opal cement inhibits consolidation of hemipelagic sediment approaching the Nankai Trough subduction zone. I analyze sediment samples from Deep Sea Drilling Project and Integrated Ocean Drilling Program sites to: 1) examine cement distribution and chemistry, and 2) determine volcanic glass sources and alteration mechanisms. I determine amorphous silica content and use backscattered electron imaging and quantitative wavelength-dispersive electron microprobe analysis to determine the distribution and source of silica cement. Four of the samples are primarily hemipelagic mud with minor amounts of volcanic glass; one sample (444-16) is a discrete ash layer with minor amounts of clay. Samples 443-30 and 444-13 are mostly clay with disseminated basaltic andesite pumice, likely sourced from the nearby Izu-Bonin Arc. Samples 442-28 and 443-34 contain rhyolitic glass chemically consistent with volcanoes from the Japanese Islands. Sample 444-16 is a rhyolitic ash layer with anomalously high FeO, chemically most closely resembling rhyolitic glass sourced from Baegdusan volcano on the border of North Korea and China. This uniquely high Fe rhyolite could be a useful marker bed in ash correlation studies. Sample 297-12 contains glass with a wide range in SiO_2, FeO, and CaO (relatively immobile elements) suggesting it is composed of glass from multiple magmatic sources contained within the same

stratigraphic interval. Due to its high clay content and fine grained glass pieces, sample 297-12 is likely the distal portion of a turbidite (Bouma sequence E) that has incorporated glass from many volcanic sources. Sample 444-16 exhibits a wide range in major element chemistry for SiO_2 and alkali elements, and has homogeneous compositions for FeO and CaO. This suggests a single volcanic source for glass that has undergone extensive post-depositional alteration. In contrast to the extensive alteration of this ash layer, there is minimal alteration of nearby disseminated glass in clay-dominated sediment with similar thermal history. We interpret the alteration of the ash layer as resulting from extensive water-rock interaction within a high permeability ash bed. Within sediment from Sites 297, 442, 443, 444, and C0006 the presence of an amorphous silica cement is detected through secondary and backscattered electron (SEM and BSE) images. The cement appears as a coating at grain contacts, filling voids in zones of clastic material, and as altered material in contact with volcanic glass shards. The observed cement appears to be mobile and sourced from these volcanic glass shards, and may be the material strengthening the sediment. The amorphous silica content of hemipelagic sediments from Sites 297, 442, 443, and 444 is higher in the Upper Shikoku Basin (USB) sediment than in the Lower Shikoku Basin (LSB), similar to results for Sites 1173, 1174, and 1177. Thus, amorphous silica cementation appears to be a common feature throughout Shikoku Basin. This cementation process may also be occurring at sites such as offshore Alaska, California, and Guatemala where conditions are favorable for the formation of sediment strengthening amorphous silica cement.

ACKNOWLEDGEMENTS

I would like to thank my advisor, Dr. Glenn Spinelli, for his encouragement, assistance and support on this project. I would also like to extend my gratitude to the members of my advisory committee, Dr. Nelia Dunbar and Dr. Peter Mozley for their time and effort, as well as Lynn Heizler for assistance with microprobe analyses. This research used samples provided by the Integrated Ocean Drilling Program (IODP). Acknowledgment is made to the Donors of the American Chemical Society Petroleum Research Fund for support of this research.

TABLE OF CONTENTS

ABSTRACT .....
ACKNOWLEDGEMENTS ii
TABLE OF CONTENTS iii
LIST OF FIGURES v
LIST OF TABLES ix
LIST OF ACRONYMS x
CHAPTER 1: SEDIMENT DISTRIBUTION AND GLASS ALTERATION 1
1.1 INTRODUCTION 1
1.2 SITE DESCRIPTION 2
1.2.1 Site 297 3
1.2.2 Sites 442, 443, 444 3
1.3 METHODS 4
1.3.1 Instrumental Techniques 4
1.3.2 Sediment Thermal History 5
1.4 RESULTS 5
1.4.1 Image Analysis 6
1.4.2 Electron Microprobe Analysis 7
1.5 DISCUSSION 12
1.5.1 Glass Sources 12
1.5.2 Sediment Dispersal 14
1.5.3 Glass Alteration 17
1.6 CONCLUSIONS 21
CHAPTER 2: GLASS ALTERATION AND SEDIMENT CEMENTATION 23
2.1 INTRODUCTION 23
2.2 SITE DESCRIPTION 24
2.2.1 Site 297 24
2.2.2 Sites 442, 443, 444 25
2.2.3 Site C0006 and C0007 26

2.4 METHODS 27
2.4.1 Amorphous Silica Content 27
2.4.2 Petrographic Analysis 28
2.5 RESULTS 29
2.5.1 Measured Amorphous Si Content 29
2.5.2 Image Analysis 30
2.6 DISCUSSION 33
2.6.1 Measured Amorphous Si 33
2.6.2 Source of Cement 34
2.6.3 Glass Alteration 35
2.7 CONCLUSIONS 37
REFERENCES 39
APPENDIX 44

LIST OF FIGURES

Figure 1.1: Location of DSDP Sites 297, 442, 443, 444, and ODP Sites 1173 and 1177 in the Shikoku Basin. p. 2

Figure 1.2: (A) Backscattered electron image of sample with high clay content and minor amount of volcanic glass. Contains both pumice pieces (P) and glass wall triple junctions (T). (B.) Image from sample 444-16 (at same scale) an ash layer with low clay content and delicate glass shards. p. 6

Figure 1.3: (A) Backscattered electron image of typical pumice piece from sample 297-12. (B) Larger pumice pieces are common in samples 443-30 and 444-13. p. 7

Figure 1.4: Total alkalis vs. silica (TAS) plot illustrating the compositional ranges of glasses from our six samples. p. 10

Figure 1.5: (A) Potassium vs. iron and (B) Calcium vs. iron variation diagrams illustrating the compositional ranges of glasses from our six samples. p. 11

Figure 1-6. Box plots of Si, Fe, Ca, and Na content (in wt%) of glass particles for our six sediment samples. p. 13

Figure 1.7: Isopach map of Late Quaternary ash sourced from B = Baegdusan with a distribution direction ~1400 km east of the source. p. 15

Figure 1.8: Thermal history for our sediment samples based on sediment accumulation rates and 1-D transient heat conduction. p. 19

Figure 2.1: Location of DSDP Sites 297, 442, 443, 444, ODP Sites 1173, 1174 and 1177, and IODP Site C0006 and C0007 in the Shikoku Basin. p. 25

Figure 2.2: Stratigraphic correlations between drill sites in Shikoku Basin and on the Nankai margin. p. 26

Figure 2.3: Site 297 sediment porosity (A; Shipboard Scientific Party, 1975) and amorphous Si content (B). p. 27

Figure 2.4: Amorphous Si content of sediment at Sites 442, 443, and 444. p. 30

Figure 2.5: Site C0006 sediment porosity (A; Shipboard Scientific Party, 2008) and amorphous Si content (B). p. 31

Figure 2.6: Representative backscattered electron (BSE) image of highly altered glass (A) with amorphous Si-rich material filling pore space (B). The sediment is dominantly clay matrix (C). Point D and surrounding bright area is a feldspar grain that is encased in volcanic glass (A). p. 31

Figure 2.7: Results of un-normalized BSE chemical analysis corresponding to points A, B, and C for sample 297-12 (Fig. 6). p. 32

Figure 2.8: Representative secondary electron microscopy (SEM) image of altered glass shard (A) with amorphous Si-rich material (B) coating clay grains (C) from sample 297-12. p. 33

Figure 2.9: Results of un-normalized BSE chemical analysis corresponding to points A and B for sample 297-12 (Fig. 9). p. 33

Figure 2.10: BSE (left) and SEM (right) images for sample 297-12 demonstrating the process of glass alteration. p. 37

Figure A1: Sample 297-12 (249 mbsf), vesiculated glass surrounding feldspar grain. p. 44

Figure A2: Sample 297-12 (249 mbsf), vesiculated glass. p. 44

Figure A3: Sample 297-12 (249 mbsf) highly dissolved vesiculated glass. p. 45

Figure A4: Sample 297-12 (249 mbsf) highly dissolved vesiculated glass. p. 45

Figure A5: Sample 442-28 (258 mbsf) large glass triple junctions and small glass fragments in clay matrix. p. 46

Figure A6: Sample 442-28 (258 mbsf) large blocky vesicular glass pieces and small glass fragments in clay matrix. p. 46

Figure A7: Sample 442-28 (258 mbsf) large glass bubble walls and small vesiculated glass in clay matrix. p. 47

Figure A8: Sample 442-28 (258 mbsf) large vesiculated glass in clay matrix. p. 47

Figure A9: Sample 443-30 (275 mbsf) vesiculated glass, small glass pieces and detrital quartz in clay matrix. p. 48

Figure A10: Sample 443-30 (275 mbsf) large glass bubble wall in clay matrix. p. 48

Figure A11: Sample 443-30 (275 mbsf) large blocky vesiculated glass, with carboniferous and siliceous microfossils in clay matrix. p. 49

Figure A12: Sample 443-30 (275 mbsf) vesiculated glass, small glass pieces and detrital quartz in clay matrix. p. 49

Figure A13: Sample 443-34 (317 mbsf) large vesiculated glass surrounding feldspar grain, minor amount of clay. p. 50

Figure A14: Sample 443-34 (317 mbsf) large vesiculated glass surrounding multiple feldspar grains, minor amount of clay. p.50

Figure A15: Sample 443-34 (317 mbsf) vesiculated glass, small glass pieces and detrital quartz in clay matrix. p. 51

Figure A16: Sample 443-34 (317 mbsf) vesiculated glass, small glass pieces and detrital quartz in clay matrix. p. 51

Figure A17: Sample 444-13 (198 mbsf) large vesiculated glass, small glass pieces and detrital quartz in clay matrix. p. 52

Figure A18: Sample 444-13 (198 mbsf) large blocky vesiculated glass and small glass pieces in clay matrix. p. 52

Figure A19: Sample 444-13 (198 mbsf) large blocky vesiculated glass, small glass pieces and detrital quarts emplaced through bioturbation in clay matrix. p. 53

Figure A20: Sample 444-13 (198 mbsf) large vesiculated glass and small glass pieces in clay matrix. p. 53

Figure A21: Sample 444-16 (226 mbsf) glass wall triple junctions and small vesiculated glass pieces with minor amount of clay. p. 54

Figure A22: Sample 444-16 (226 mbsf) glass wall triple junctions and vesiculated glass pieces with minor amount of clay. p. 54

Figure A23: Sample 444-16 (226 mbsf) fine grained glass wall triple junctions and vesiculated glass pieces in clay matrix. p. 55

Figure A24: Sample 444-16 (226 mbsf) glass wall triple junctions and vesiculated glass pieces in clay matrix. p. 55

LIST OF TABLES

Table 1.1: Major-element chemistry of volcanic glass in Shikoku Basin
p. 8

LIST OF ACRONYMS

BSE – Backscattered electron imaging

DSDP – Deep Sea Drilling Project

IODP – Integrated Ocean Drilling Program

ODP – Ocean Drilling Program

SEM – Secondary electron imaging

CHAPTER 1: SEDIMENT DISTRIBUTION AND GLASS ALTERATION

1.1 INTRODUCTION

Chemical and morphological analyses of volcanic glass fragments are used to determine volcanic source area, size and timing of magmatic events, stratigraphic correlations, and sediment dispersal patterns (Huang, 1980; Perkins et al., 1995; Shane et al., 1996; Haberle and Lumley, 1998; Katoh et al., 2000; Schneider et al., 2001). Generally, these studies compare the chemical composition of discrete ash layers or disseminated glass fragments within sediment to the chemistry of known volcanic sources or corollary samples. Typically, the geochemical analyses used for correlation are carried out on individual glass shards using microbeam techniques in order to avoid the problem of sample contamination. In order to interpret major element chemical compositions of volcanic glass it is necessary to understand both controls on the composition of erupted material and the processes that affect their composition during diagenesis. Fractional crystallization in a magma chamber causes an evolution (from mafic to felsic) of the eruption product. Volcanic material from "primitive" or basaltic magmatic systems have low Si and alkali element content, high CaO and FeO content, whereas the composition of more evolved magmas are enriched in SiO_2 and alkali elements;and are lower in CaO and FeO. The mobility of elements within volcanic glass during post-eruptive hydration processes is highly variable; it is controlled by temperature, water-rock interaction, and the composition of glass and water (Hajash and Chandler, 1981). Volcanic glass readily alters to more stable phases, such as smectite or other clay minerals. This alteration process involves the mobilization of elements; Na_2O and K_2O are the first elements to be leached from volcanic glass (Cerling et al., 1985).

Here we use the depletion of these alkali elements as an indicator for glass alteration. Most other elements are considerably less mobile than Na_2O and K_2O (Stefansson and Gislason, 2001; Gislason, 2008). We use SiO_2, FeO, and CaO (i.e. relatively immobile elements) compositions to identify volcanic source area and sediment mixing.

Glass analyses have been successfully applied to a range of geologic problems throughout the Shikoku Basin and surrounding Japanese islands. Extensive volcanism in the area and preservation of volcanic deposits allows chemical and stratigraphic correlations of distal tephra layers to their eruptive sources (Machida, 1999). For example, glass chemistry data coupled with image analyses and sedimentary structures have been used to infer the timing, source, and mechanism of glass transport for ash beds of the Miura-Boso Peninsulas, Japan (Lee and Ogawa, 1998). In this study, we discuss the results of analyses for six sediment samples from the Shikoku Basin in order to highlight the utility of glass chemistry when interpreting depositional and post-depositional processes of sediment containing volcanic material within the submarine environment.

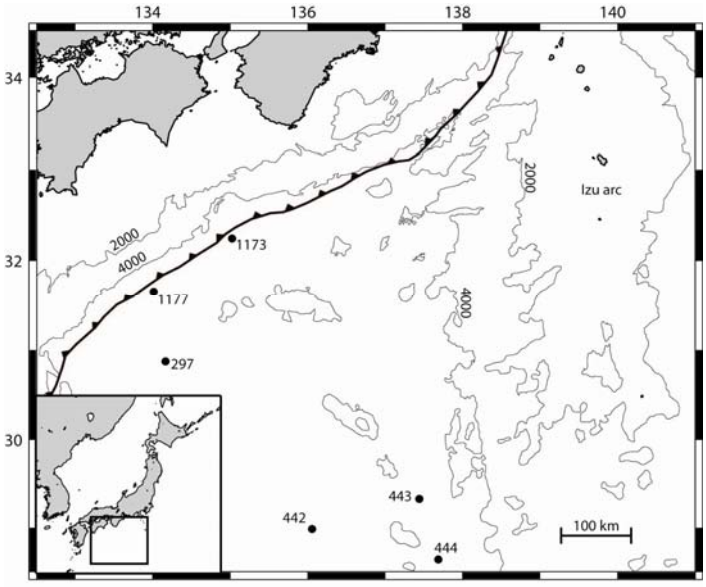

Figure 1.1: Location of DSDP Sites 297, 442, 443, 444, and ODP Sites 1173 and 1177 in the Shikoku Basin. Thin lines are bathymetry in meters. Barbed line is Nankai Trough subduction zone deformation front.

1.2 SITE DESCRIPTION

We examined sediment

samples from four Deep Sea Drilling Project (DSDP) sites offshore southern Japan in Shikoku Basin (Fig. 1.1). The lithosphere in Shikoku Basin was created by spreading along a ridge (spreading stopped ~15 Ma); the Kinan seamount chain (Fig. 1.1) delineates this fossil spreading center (Chamot-rooke et al., 1987; Okino et al., 1994). The Shikoku Basin is flanked to the east by the Izu-Bonin Arc and to the west by the Kyushu-Palau Ridge.

1.2.1 Site 297

Site 297 is ~100 km seaward of the Nankai Trough subduction zone on ~23 Ma crust. The estimated total sediment thickness is 780 m; 680 m were drilled on DSDP Leg 31 (Shipboard Scientific Party, 1975). The sediments are primarily hemipelagic mud with ash,

silt, and sand interbeds (Shipboard Scientific Party, 1975). We examine a sample from 249 meters below seafloor (mbsf) within a unit consisting of claystone with minor ash and fossils. This interval likely is equivalent stratigraphically to the upper Shikoku Basin facies described at Ocean Drilling Program sites in the region (Shipboard Scientific Party, 2001b; 2001d). The sediment from which our sample 297-12 was collected is dominantly (~85%) clay minerals with ~3% volcanic glass (Shipboard Scientific Party, 1975).

1.2.2 Sites 442, 443, 444

Sites 442, 443, and 444 are approximately 400 km from the trench on slightly younger crust than Site 297; they are closer to the fossil spreading ridge (Fig. 1.1). The sediment at Sites 442 and 444 is ~410 m thick; at Site 443 there is ~580 m of sediment (Shipboard Scientific Party, 1980a; 1980b, 1980c). At all three sites the sediment consists

of hemipelagic mud with some distinct ash layers and some disseminated ash. We examined one sample from Site 442 (258 mbsf), described in smear slides as ~91% clay minerals and ~2% volcanic glass(Shipboard Scientific Party, 1980a). We examined two samples from Site 443: 275 mbsf, ~63% clay minerals and ~12% volcanic glass; and 317 mbsf, ~74% clay minerals and ~13% volcanic glass Finally, we examined two samples from Site 444: 198 mbsf, ~60% clay minerals and 7% volcanic glass; and 226 mbsf, ~5% clay minerals and ~95% volcanic glass (Shipboard Scientific Party, 1980c).

1.3 METHODS

1.3.1 Instrumental Techniques

Samples were examined using backscattered electron (BSE) imaging on a Cameca SX-100 microprobe at New Mexico Tech. Operating conditions for the microprobe were 15kV acceleration voltage and 10 nA beam current. Vacuum and surface impregnation techniques were used in order to preserve the texture and structure of the samples during lapping and polishing. Slides were polished and then evaporatively coated with carbon and analyzed using quantitative elemental analysis of selected phases using wavelength-dispersive spectrometers (White et al., Submitted). Most glass analyses were conducted using a beam diameter of 10 μm, due to the small size of the shards; where possible a 15 or 20 μm beam was used.

Glass shards were quantitatively analyzed to determine the abundance of SiO_2, Al_2O_3, TiO_2, FeO, MnO, MgO, SO_2, CaO, Cl, Na_2O, and K_2O. Count times of 20 seconds were used for all elements except SO_2 and Cl, which were counted for 30 seconds. Standard reference materials of feldspars, amphiboles, and glasses were analyzed at the beginning and end of each analysis in order to determine analytical

accuracy and precision, as well as to monitor instrument calibration. A total of 138 individual volcanic glass fragment and pumice pieces were analyzed from six sediment samples with an average of 24 glass pieces analyzed from each sample. Sample totals for the glass analyses are ~95%, with low totals caused by glass hydration (Scheidegger et al., 1978; Reed, 1996). Therefore the data were normalized to 100% to allow better comparison among samples. Analyses with totals <85% were discarded.

1.3.2 Sediment Thermal History

We estimate the thermal history for each sediment sample based on the sediment accumulation history for each site and 1-D transient heat conduction between the basalt basement and the seafloor (White et al., Submitted). Sedimentation rates for Sites 442, 443, and 444 are constrained by biostratigraphy (Shipboard Scientific Party, 1980a; 1980b; 1980c). For site 297, which has limited age constraints, we apply sedimentation rates for the lower and upper Shikoku Basin facies from the nearest Ocean Drilling Program (ODP) site (1177; Shipboard Scientific Party, 2001d). We follow the method applied for estimating thermal histories of Site 1173 and 1177 sediment (Spinelli et al., 2007). The seafloor is a constant temperature boundary; heat flux into the base of the sediment column decreases as the lithosphere conductively cools over time.

1.4 RESULTS

We use BSE images to compare glass morphology, clay content, and grain size distributions within each sample. Grain sizes were measured for each quantitatively analyzed point to insure proper beam size was applied for glass composition analysis and to draw sedimentological inferences based on grain size distributions. The mineralogy,

chemistry and morphology of these samples are applied to interpreting the sedimentary, diagenetic, and volcanic history of the area.

1.4.1 Image Analysis

There is a distinct lack in clay content for sample (444-16) compared to all other samples examined (Fig. 1.2). Clay-dominated samples (~60-90% clay) contain ~5-15% volcanic glass fragments, and minor amounts of volcanic rock fragments and biogenic tests disseminated throughout the sediment (Fig. 1.2a). In contrast the ash layer (444-16) is ~95% volcanic glass and ~5% clay; there is a distinct lack of biologic material (Fig. 1.2b). Glass within samples 297-12 (Fig. 1.3a), 443-30, and 444-13 (Fig. 1.3b) are primarily vesiculated

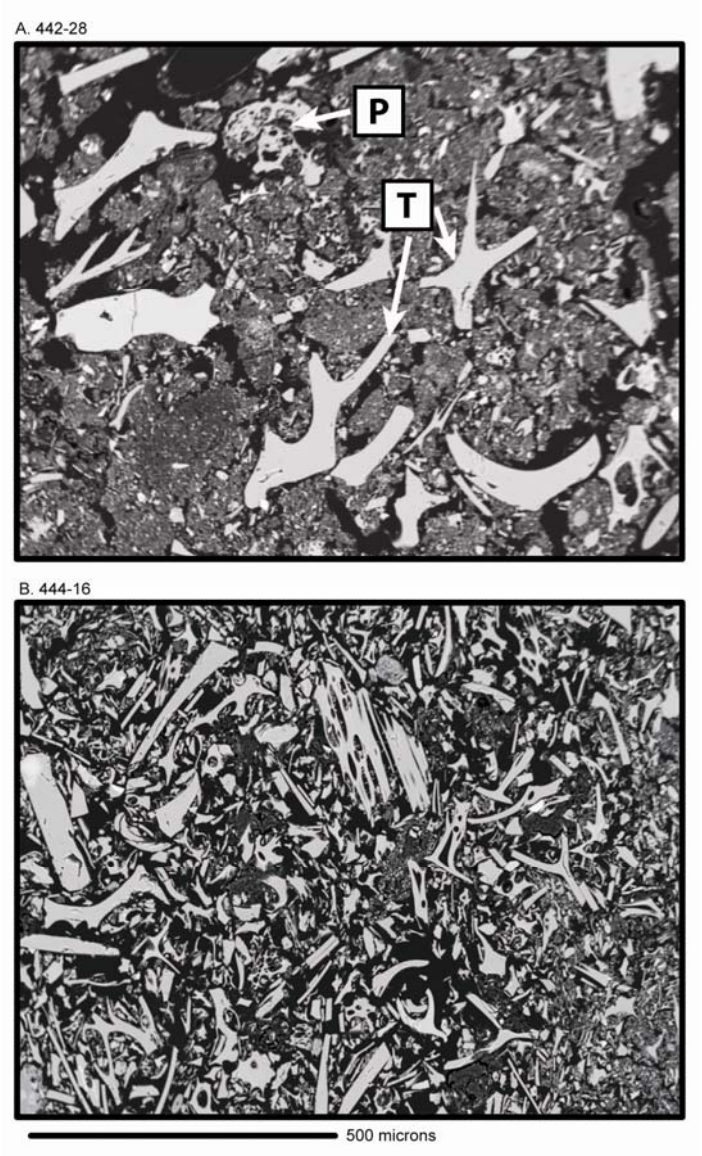

Figure 1.2: (A) Backscattered electron image of sample with high clay content and minor amount of volcanic glass. Contains both pumice pieces (P) and glass wall triple junctions (T). (B.) Image from sample 444-16 (at same scale) an ash layer with low clay content and delicate glass shards.

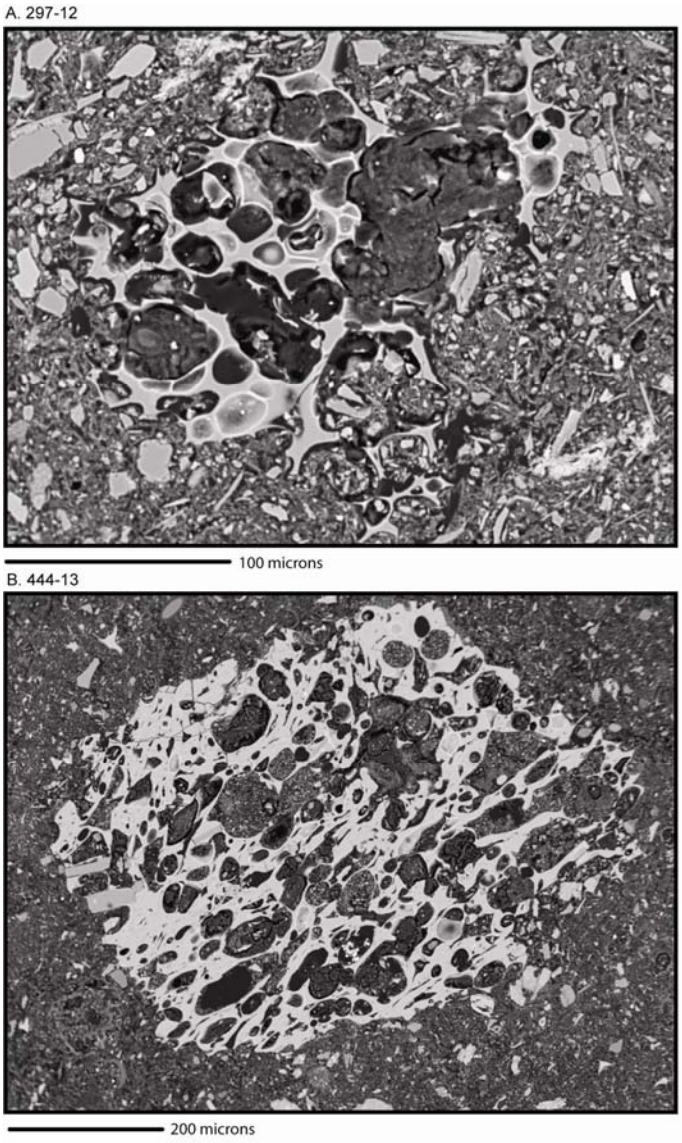

Figure 1.3: (A) Backscattered electron image of typical pumice piece from sample 297-12. (B) Larger pumice pieces are common in samples 443-30 and 444-13.

glass fragments, while samples 442-28 and 443-34 are composed of both bubble wall shards and vesiculated glass (Fig. 1.2a). Glass morphology for sample 444-16 is similar to that of samples 442-28 and 443-34, but the 444-16 glass shards are more delicate and smaller than those found within the five other samples (Fig. 1.2b).

1.4.2 Electron Microprobe Analysis

The normalized results of the electron microprobe analyses are given in Table 1-1. Glass populations from each sediment sample form individual clusters on a total alkali versus silica (TAS) plot (Fig. 1.4). Glass from samples 442-28, 443-30, 443-34, and 444-13 fall primarily in tight clusters (Fig. 1.4); although, five shards from sediment sample 443-30 occur well outside the otherwise tight basaltic andesite cluster (i.e. dacite to rhyolite). Glass chemistry distributions from 297-12 and 444-16 are more

Table 1.1: Major-element chemistry of volcanic glass in Shikoku Basin

Sample	SiO_2	SO_2	TiO_2	Al_2O_3	MgO	CaO	MnO	FeO	Na_2O	K_2O
297-12* (248.95 mbsf, 3.20 Ma)										
	67.97	0.07	0.45	16.22	0.90	4.81	0.07	3.81	3.76	1.43
	71.80	0.03	0.49	14.65	0.92	3.29	0.07	3.25	3.18	1.88
	64.18	0.02	0.50	18.49	0.82	6.42	0.10	3.86	4.09	1.23
	70.60	0.02	0.47	15.23	0.74	3.89	0.10	3.40	3.50	1.78
	53.09	0.01	1.03	13.84	5.36	9.92	0.25	13.39	2.52	0.36
	76.93	0.02	0.30	12.49	0.34	1.98	0.07	1.73	3.74	2.20
	68.46	0.01	0.51	16.74	0.51	5.00	0.04	3.14	3.93	1.43
	75.72	0.02	0.12	14.07	0.23	1.58	0.03	2.14	2.63	3.24
	70.82	0.02	0.53	14.52	0.98	3.56	0.12	3.49	3.93	1.70
	77.13	0.01	0.26	12.70	0.47	1.82	0.09	1.99	3.11	2.19
	71.36	0.05	0.47	14.45	1.02	3.54	0.08	3.42	3.50	1.78
	76.66	0.03	0.30	13.00	0.42	2.05	0.08	2.01	2.88	2.19
	68.29	0.03	0.61	15.62	1.33	4.32	0.07	4.38	3.46	1.61
	70.66	0.01	0.47	15.40	0.77	3.93	0.05	2.97	3.65	1.81
442-28¥ (258.13 mbsf, 14.08 Ma)										
	78.81	0.00	0.06	12.00	0.02	0.59	0.03	0.90	2.64	4.77
	79.21	0.01	0.10	11.74	0.01	0.60	0.05	0.94	2.61	4.55
	78.22	0.00	0.08	11.83	0.02	0.60	0.00	0.92	2.84	4.87
	78.26	0.00	0.06	11.98	0.02	0.60	0.02	1.01	2.80	4.79
	78.68	0.01	0.13	12.11	0.02	0.64	0.01	0.97	2.63	4.58
	79.32	0.00	0.04	12.07	0.01	0.58	0.05	1.04	2.24	4.31
	78.33	0.02	0.12	11.89	0.01	0.60	0.03	0.99	2.57	5.19
	78.40	0.04	0.13	11.96	0.02	0.62	0.03	1.04	2.73	4.86
	78.67	0.00	0.13	11.68	0.02	0.57	0.02	0.89	2.29	5.47
	78.82	0.01	0.10	11.89	0.02	0.64	0.00	1.06	2.08	5.17
	79.14	0.00	0.05	11.90	0.01	0.57	0.02	0.83	2.58	4.61
	78.67	0.00	0.06	11.92	0.03	0.65	0.03	0.96	2.57	4.99
	79.12	0.00	0.10	11.94	0.03	0.62	0.00	0.93	2.43	4.58
	78.74	0.00	0.09	11.98	0.03	0.61	0.00	0.96	2.58	4.77
	78.28	0.04	0.06	11.81	0.03	0.60	0.02	1.05	2.60	5.23
	78.93	0.00	0.11	11.68	0.04	0.61	0.04	0.99	2.74	4.79
	78.71	0.00	0.13	11.75	0.03	0.62	0.04	0.97	2.64	5.04
	79.71	0.00	0.05	11.76	0.03	0.52	0.05	0.92	2.22	4.40
	67.55	0.13	0.86	14.17	1.42	3.99	0.07	5.14	2.79	3.20
	53.26	0.02	1.13	16.39	3.95	10.49	0.17	11.69	2.21	0.36
	78.87	0.01	0.11	11.91	0.03	0.61	0.05	0.90	2.61	4.50
	77.03	0.02	0.02	12.98	0.18	0.65	0.06	1.22	2.18	4.79
	59.29	0.00	1.04	13.73	3.88	8.02	0.22	10.45	1.96	0.92
	71.70	0.00	0.15	15.64	0.02	1.35	0.06	1.62	5.09	4.01
	79.92	0.00	0.10	11.83	0.02	0.60	0.03	0.88	2.29	4.21
	78.92	0.00	0.07	11.95	0.01	0.59	0.02	1.00	2.41	4.78
	81.77	0.00	0.08	12.15	0.02	0.62	0.00	0.97	0.66	3.53
	78.98	0.00	0.09	11.93	0.02	0.58	0.00	0.90	2.54	4.87
	78.12	0.02	0.09	12.05	0.02	0.63	0.07	1.03	2.61	5.05
	79.16	0.01	0.09	11.95	0.04	0.63	0.05	0.98	2.25	4.55
	79.29	0.03	0.11	11.84	0.01	0.56	0.02	0.99	2.27	4.62
	79.82	0.00	0.12	11.86	0.00	0.58	0.02	0.92	2.33	4.20
	78.63	0.00	0.01	12.82	0.03	0.64	0.01	0.89	2.67	4.15
	78.87	0.00	0.09	12.01	0.01	0.58	0.02	1.09	2.58	4.46
	78.68	0.00	0.09	11.85	0.02	0.62	0.06	0.98	2.35	5.17
	78.56	0.01	0.10	12.00	0.03	0.62	0.02	1.00	2.48	4.92
	79.05	0.01	0.12	12.26	0.05	0.80	0.04	1.30	2.19	4.09
	79.41	0.03	0.08	11.87	0.03	0.53	0.04	0.99	2.35	4.49
	72.42	0.04	0.59	12.05	0.71	4.16	0.17	6.28	2.42	0.45
443-30§ (274.96 mbsf, 9.55 Ma)										
	55.81	0.04	1.10	14.49	4.06	8.95	0.24	12.14	2.52	0.36
	55.82	0.09	1.07	14.39	3.90	8.98	0.15	12.32	2.55	0.36
	56.59	0.01	1.05	14.23	3.79	8.59	0.22	12.01	2.65	0.36
	56.04	0.06	0.97	14.60	4.17	8.55	0.24	12.01	2.35	0.38
	56.88	0.03	0.99	14.37	3.82	8.74	0.26	11.86	2.41	0.37
	75.86	0.01	0.31	14.57	0.43	1.39	0.02	1.38	2.63	3.00
	56.47	0.05	1.09	14.27	3.86	8.71	0.21	12.24	2.56	0.35
	56.18	0.07	1.07	14.18	3.96	8.82	0.25	12.19	2.72	0.37
	56.30	0.01	1.10	14.18	3.93	8.67	0.20	12.38	2.46	0.37
	79.36	0.03	0.42	11.93	0.43	2.34	0.13	2.13	2.46	0.57
	79.44	0.03	0.28	12.14	0.41	1.72	0.11	1.93	2.17	1.29
	78.87	0.00	0.39	12.17	0.42	2.31	0.13	2.32	2.48	0.58
	54.36	0.02	0.95	8.10	11.18	8.85	0.33	14.63	1.04	0.23
	56.83	0.02	0.99	13.88	4.16	8.83	0.20	12.24	2.32	0.33
	66.50	0.25	0.92	14.93	1.09	3.63	0.14	4.85	4.52	2.49
	57.61	0.00	0.94	14.98	3.56	9.43	0.18	10.11	2.64	0.32

443-34† (317.39 mbsf, 12.03 Ma)									
74.03	0.04	0.45	13.49	0.53	3.34	0.22	4.18	2.72	0.69
74.81	0.12	0.46	13.24	0.52	3.18	0.15	4.01	2.30	0.84
74.35	0.02	0.38	13.45	0.45	3.22	0.19	3.88	2.87	0.76
74.52	0.00	0.45	13.44	0.30	3.31	0.12	4.03	2.69	0.69
75.32	0.00	0.52	12.99	0.30	3.21	0.15	4.10	2.36	0.66
78.34	0.04	0.42	11.60	0.40	2.80	0.17	3.44	1.87	0.62
76.05	0.01	0.45	12.90	0.29	3.32	0.16	4.04	1.83	0.65
75.53	0.02	0.50	12.64	0.53	3.43	0.12	3.97	2.08	0.76
75.42	0.01	0.40	12.74	0.35	3.17	0.18	3.65	2.91	0.81
75.10	0.03	0.45	12.77	0.50	3.23	0.14	3.97	2.65	0.70
75.15	0.00	0.56	12.86	0.58	3.33	0.18	5.11	1.36	0.57
75.44	0.00	0.43	12.73	0.51	3.11	0.21	3.74	2.65	0.85
75.40	0.01	0.45	12.65	0.49	3.10	0.18	3.90	2.49	0.73
76.31	0.00	0.47	12.66	0.42	3.29	0.16	3.99	1.74	0.62
73.01	0.02	0.50	13.76	0.46	4.13	0.16	4.45	2.43	0.67
74.58	0.08	0.46	12.21	0.70	3.65	0.17	4.32	2.51	0.74
74.99	0.01	0.41	12.81	0.64	3.16	0.17	4.25	2.24	0.83
73.12	0.01	0.66	12.52	0.86	3.99	0.13	5.29	2.25	0.55
72.37	0.02	0.68	12.49	0.88	4.21	0.19	5.46	2.66	0.55
74.08	0.03	0.59	12.21	0.83	3.65	0.13	4.88	2.40	0.61
76.09	0.10	0.49	12.62	0.50	2.22	0.10	2.27	2.18	3.02
71.21	0.01	0.67	13.03	1.10	4.43	0.15	5.63	2.79	0.54
75.60	0.02	0.45	12.80	0.47	3.43	0.17	3.99	2.19	0.62
74.82	0.01	0.42	12.73	0.55	3.38	0.17	4.15	2.41	0.72
75.23	0.01	0.34	12.94	0.65	3.10	0.21	3.86	2.32	0.86
74.22	0.01	0.45	12.95	0.51	3.64	0.16	3.53	3.41	0.69
74.31	0.00	0.43	13.40	0.50	3.55	0.21	4.19	2.44	0.58
75.95	0.02	0.51	12.82	0.49	3.15	0.18	3.99	1.91	0.65
75.71	0.01	0.41	13.29	0.48	3.30	0.11	3.90	1.86	0.66
75.19	0.01	0.38	12.93	0.49	3.23	0.17	4.00	2.68	0.66
75.14	0.01	0.36	12.92	0.49	3.16	0.18	3.95	2.84	0.73
75.42	0.02	0.40	12.76	0.44	3.33	0.17	3.85	2.36	0.72
76.21	0.03	0.45	12.91	0.53	3.36	0.19	4.02	1.44	0.63
444-13€ (197.92 mbsf, 11.75 Ma)									
55.65	0.06	1.05	15.39	3.79	8.85	0.20	11.49	2.57	0.55
54.05	0.18	1.04	15.31	4.33	9.46	0.32	12.02	2.49	0.46
54.28	0.11	1.08	15.23	4.26	9.47	0.26	11.81	2.56	0.53
55.03	0.13	1.05	14.93	4.42	8.85	0.24	12.25	2.16	0.54
55.80	0.08	1.04	15.03	3.94	8.87	0.24	11.62	2.59	0.53
54.90	0.12	1.06	14.77	3.93	8.83	0.23	12.05	2.96	0.56
56.05	0.05	1.05	13.92	4.70	9.34	0.30	11.87	1.91	0.49
55.02	0.05	1.08	14.13	4.61	8.83	0.23	11.37	3.93	0.48
56.96	0.07	1.03	15.14	3.74	8.66	0.27	11.08	2.26	0.56
444-16£ (226.42 mbsf, 13.29 Ma)									
80.65	0.01	0.25	11.97	0.01	0.25	0.14	3.56	0.82	2.07
71.14	0.03	0.25	14.89	0.07	1.40	0.14	3.38	4.03	4.46
74.97	0.03	0.33	11.63	0.00	0.80	0.13	4.19	2.75	4.88
75.79	0.00	0.18	11.25	0.00	0.22	0.09	3.28	4.11	4.89
75.47	0.05	0.28	12.20	0.07	0.80	0.16	4.18	2.74	3.88
76.13	0.00	0.19	11.23	0.33	0.16	0.14	3.34	3.72	4.58
69.03	0.03	0.38	15.36	0.24	1.50	0.08	3.82	5.29	4.19
76.71	0.01	0.26	11.51	0.00	0.21	0.05	3.50	3.11	4.37
73.57	0.03	0.41	13.61	0.13	1.33	0.22	5.31	1.26	3.92
74.54	0.03	0.18	11.79	0.32	0.31	0.11	3.65	3.55	4.99
70.58	0.00	0.44	15.75	0.24	1.61	0.10	3.83	2.94	4.37
75.83	0.00	0.24	11.97	0.02	0.41	0.19	3.85	2.98	4.27
75.62	0.14	0.25	11.16	0.21	0.15	0.12	3.58	4.22	3.96
75.96	0.01	0.21	11.86	0.00	0.21	0.11	3.46	3.47	4.58
71.99	0.00	0.32	13.00	0.42	0.86	0.18	4.40	4.04	4.52
76.42	0.01	0.17	11.67	0.00	0.28	0.11	3.67	3.17	4.31
68.31	0.00	0.44	15.46	0.24	1.60	0.10	4.27	4.30	5.13
77.25	0.02	0.19	11.33	0.00	0.21	0.08	3.37	3.16	4.06
70.37	0.04	0.67	14.32	0.22	2.02	0.27	6.32	2.26	3.31
76.74	0.02	0.21	11.28	0.00	0.24	0.09	3.35	3.38	4.44
77.48	0.02	0.20	11.42	0.00	0.19	0.08	3.42	2.90	4.09
73.17	0.00	0.30	14.92	0.06	1.36	0.15	3.46	2.16	4.16
73.18	0.05	0.36	13.21	0.09	1.15	0.24	5.10	2.05	4.33
77.29	0.00	0.28	11.71	0.00	0.22	0.03	2.76	3.29	4.24
77.57	0.02	0.23	11.65	0.00	0.24	0.14	3.71	2.75	3.54
74.40	0.00	0.25	11.67	0.00	0.19	0.10	3.48	4.41	5.27
74.97	0.00	0.24	11.46	0.00	0.19	0.07	3.59	4.28	4.95

Note: Samples normalized to 100 % to account for lower probe count due to hydration.

Sample size: *n=14 ¥n=39 §n=16 †n=33 €n=9 £n=27

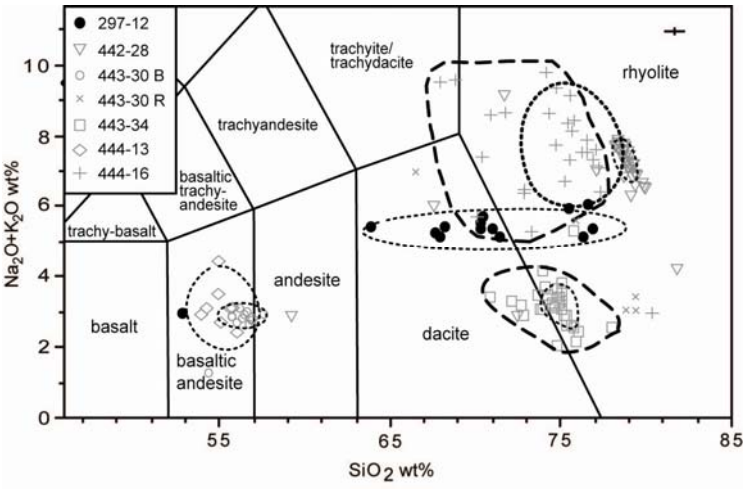

Figure 1.4: Total alkalis vs. silica (TAS) plot illustrating the compositional ranges of glasses from our six samples (field boundaries and nomenclature from Le Maitre, 1989). Clusters are encircled by a dotted line on the 50% data density contour (data density within dotted line > 1/2 maximum density for cluster). Sample 442-28 and 443-34 have large regions of low data density and are encircled by a second dashed line to highlight the range in values. Sample 297-12 has a wide range in SiO2 and little variability in alkali content. Sample 444-16 has variability of both SiO2 and alkali elements. Sample 443-30 has been broken up into two populations, basaltic (B) and rhyolitic (R). Cross in upper right shows precision of measurements determined by analysis of standards.

variable. To discriminate glass sources and aid with interpretation of processes, for each compositional cluster we determined the data density and plotted the 50% density contour (i.e. encircled fields have density of data points ≥1/2 maximum density for the cluster) (Fig. 1.4). The glass chemistry distributions from sediment samples 443-34 and 444-16 have fairly large regions with low data density; in these two cases, a second broader field was drawn to highlight the total range in compositions.

Glass compositions in the six sediment samples range from basaltic andesite to rhyolite and there is a wide range of alkali contents between the individual rhyolitic samples. Samples 443-30 and 444-13 contain primarily basaltic andesite glass and overlap one another in fairly tight compositional clusters. Glasses in sediment samples 442-28 and 443-34 are mostly rhyolitic in composition; their distributions consist of a tight central cluster and modest tail regions with low data density (Fig. 1.4). The

distribution of glass compositions from sediment samples 297-12 and 444-16 are quite different from those for other samples and each other. Glasses from 297-12 show a large range in SiO_2 content (~54% to ~76%); most are spread over a range from dacite to rhyolite with very little consistency of glass chemistry from shard to shard (the distribution is a broad plateau). There is little variation in total alkali content in the 297-12 glasses (Fig. 1.4). The glasses from 444-16 are dominantly rhyolite; their compositional distribution is much wider (in both silica and total alkali contents) than those from other sediments sampled. Further differences in glass composition distributions are examined in K_2O vs. FeO and CaO vs. FeO plots (Fig. 1.5).

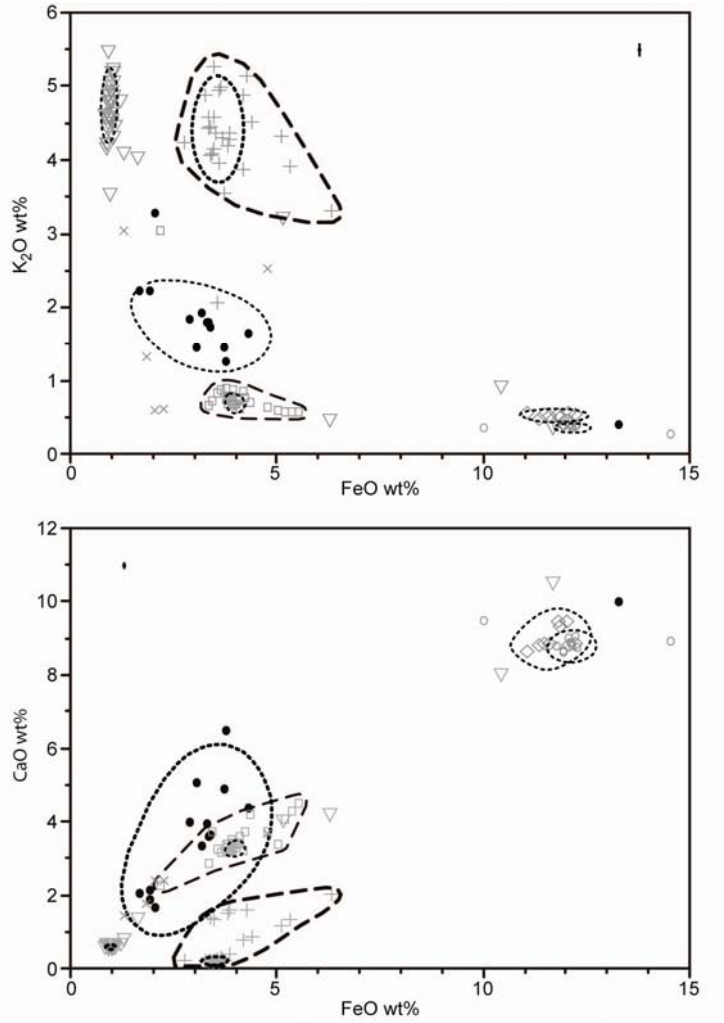

Figure 1.5: (A) Potassium vs. iron and (B) Calcium vs. iron variation diagrams illustrating the compositional ranges of glasses from our six samples. Symbols and lines are the same as in Figure 4. Sample 444-16 exhibits anomalously high Fe for a rhyolite.

As with Figure 1.4, the 50% density contour for each cluster is shown; additional broad fields are shown for samples 443-34 and 444-16. The distributions highlight the

compositional homogeneity of glass in samples 442-28, 443-30, 443-34, and 444-13 compared to the diffuse distributions for samples 297-12 and 444-16, particularly with respect to K_2O vs FeO. Sample 444-16 glasses have anomalously high FeO content for a rhyolite (Fig. 1.5b). The high FeO content for the 444-16 glasses shift them well off the trend in CaO versus FeO content displayed by glasses from all the other samples (Fig. 1.5b). The wide range in chemical compositions for sample 444-16 is not expressed for all elements. Elements FeO and CaO (Fig. 1.5b) have a relatively tight cluster, compared to SiO_2 (Fig. 1.4), K_2O (Fig. 1.5a), and Na_2O (Fig. 1.6) contents which are quite diffuse. This concentration of FeO and CaO as well as the wide range in SiO_2, K_2O, and Na_2O may be used to identify the processes that affected the ash layer contained within sample 444-16.

For the six glass composition clusters, we use box plots to compare distributions of Si, FeO, CaO, and Na_2O content (Fig. 1.6). Their interquartile ranges (IQR) for SiO_2 content are <1.18 wt% and for CaO content are <0.51 wt%. Samples 444-16 and 297-12 have a wide range in compositions. The IQR for Si content in 444-16 is 3.40 wt% and in 297-12 is 6.40 wt%. For Na_2O, the distribution for sample 444-16 is much broader (IQR=1.29 wt%, range=4.47 wt%) than for sample 297-12 (IQR=0.63 wt%, range=1.57 wt%) as well as all other samples.

1.5 DISCUSSION

1.5.1 Glass Sources

Although no direct correlation to individual eruptive events can be made, the rhyolite and dacite glass compositions from samples 297-12, 442-28, 443-30, and 443-34 are consistent with arc volcanics from the Japanese Islands (Furuta and Arai, 1980;

Pouclet et al., 1986). The source of the basaltic andesites in samples 443-30 and 444-13 is likely closer to the drilling sites than the felsic source; the large basalt andesite pumice pieces are likely transported a shorter distance compared to the smaller rhyolitic glass (Furuta and Arai, 1980). The major element chemistry of the sample 443-30 and 444-13 glasses is consistent with similar basaltic andesites sourced from the Izu-Bonin Arc (Yuasa and Nohara, 1992).

The diagnostically high FeO content of rhyolitic glass (Hildreth, 1981; Machida, 1999) of sample 444-16 (Fig. 1.5b) may help identify the source volcano for the ash layer. Rhyolites that are

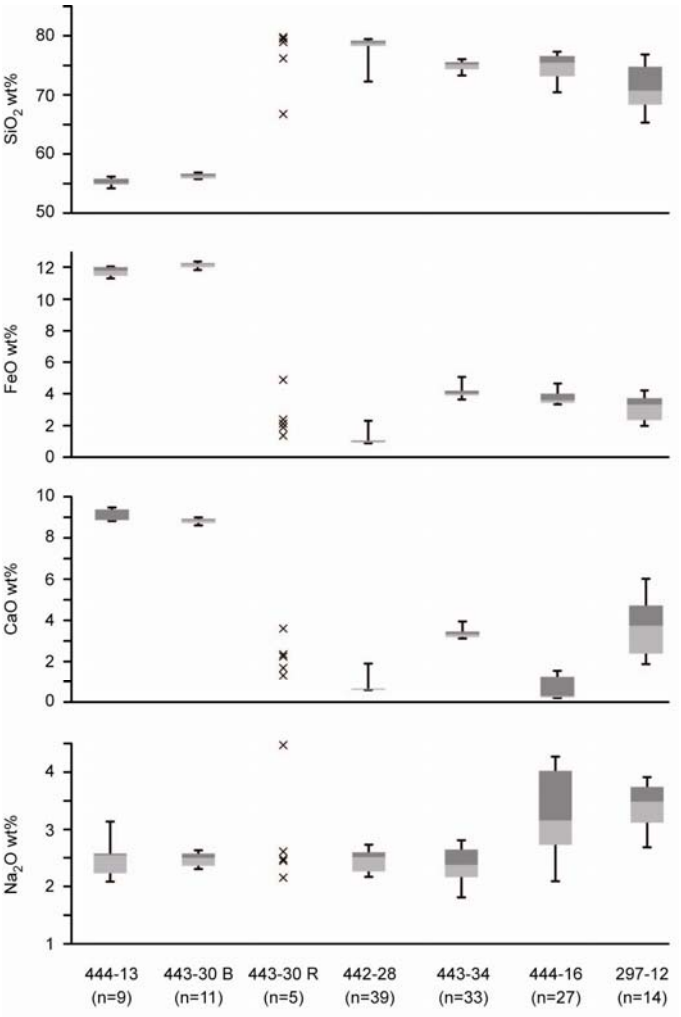

Figure 1.6: Box plots of Si, Fe, Ca, and Na content (in wt%) of glass particles for our six sediment samples (number of glass particles analyzed indicated below sample ID; 138 samples total). Median value is at transition from light to dark gray within each box. Top and bottom of boxes are 75th and 25th percentile, respectively. The 90th and 10th percentile are indicated by ends of lines extending from boxes. Samples 297-12 and 444-16 show significantly greater ranges in element composition compared to the other samples.

sourced from different volcanoes can have very different chemical compositions that can be used to fingerprint a source (Sarna-Wojcicki et al., 1984). There are very few volcanic sources near the Shikoku Basin that produce rhyolitic glass having FeO content similar to sample 444-16. Within the region, Baegdusan on the border of North Korea and China produces glass with major element chemistry most similar to that of sample 444-16 (Machida, 1999). However, Baegdusan has been active only since the early Pleistocene (Machida, 1999) while the 444-16 sediment sample was deposited much earlier (~12 Ma). Although volcanic regions have been shown to generally overtime have, more similar than not, chemically characteristic eruptions (Sarna-Wojcicki et al., 1984; Self et al., 1986; Perkins et al., 1995). Furthermore, the described transport direction for ash is due east where as Site 444 is located ~150^{o} to the southeast. The distance between Baegdusan volcano and the sediment core is 1700 km, which is ~300km beyond the known transport distance for volcanic ash sourced from Baegdusan (1400km) (Machida, 1999), but is not an unreasonable distance. A minor change in wind direction of ~60^{o} could easily transport material sourced from Baegdusan volcano out to Site 444 within the Shikoku Basin (Fig. 1.7). If the high FeO content of rhyolitic glass observed at Baegdusan volcano is indicative of volcanoes in that region, the volcanic ash in the 444-16 could be derived from another, related volcano in the same volcanic region. However, the limited information available on geochemistry of this volcanic area prevents any further correlation to be made.

1.5.2 Sediment Dispersal

Glasses in sample 297-12 likely are derived from multiple magmatic sources; all other samples apparently reflect single ash sources. Sample 297-12 glass shards have

large ranges in SiO_2, FeO, and CaO contents with very little variation of alkali elements (Fig. 1.4). SiO_2, FeO, and CaO are not strongly affected by glass alteration (Stefansson and Gislason, 2001; Gislason, 2008). These components are relatively homogeneous within all samples except 297-12, suggesting a process unique to 297-12 is responsible for its deposition. The wide range in relatively immobile elements (SiO_2, FeO, CaO) (Fig. 1.4, 1.5, and 1.6) and the homogeneity of total alkali elements (K_2O and Na_2O) (Fig. 1.4) suggests glass from multiple magmatic sources is contained within sample 297-12 and has undergone little alteration.

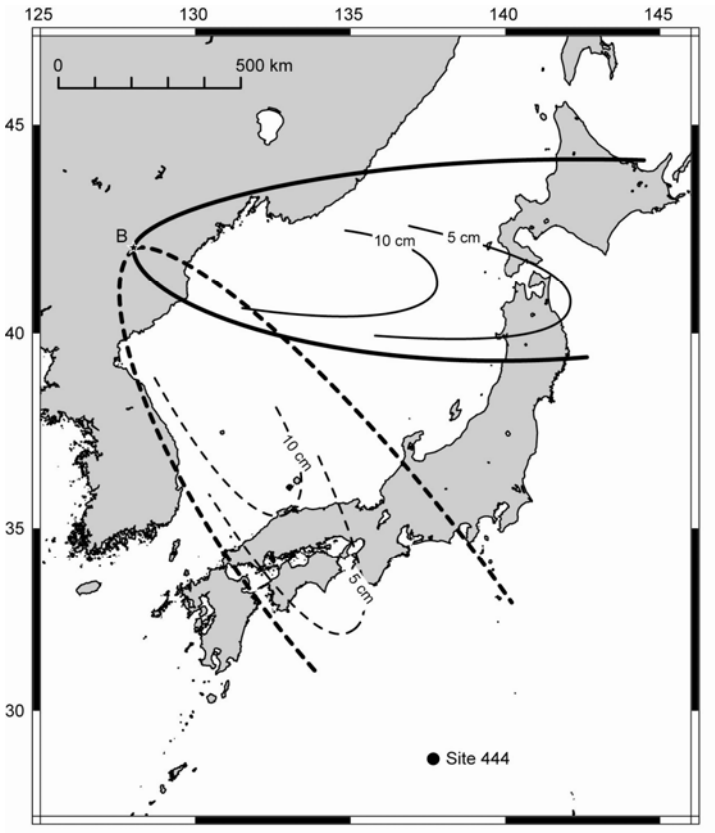

Figure 1.7: Isopach map of Late Quaternary ash sourced from B = Baegdusan with a distribution direction ~1400 km east of the source (solid lines; Machida, 1999). With wind direction shifted 53o to the southeast, ash from the Baegdusan region could be transported to Shikoku Basin (hypothesized ash distribution in dashed lines).

The chemistry as well as the age of sample 297-12 is consistent with that of a turbidite containing glass from multiple magmatic sources deposited during a time of known turbidite deposition. Ash from multiple events can be deposited on the continental margin as discrete event beds before being carried out into the basin via

turbidites or bottom currents (Norin et al., 1958; Huang, 1980; Ogawa, 1998; Schneider et al., 2001). Seafloor topography has been shown to strongly influence the distribution of turbidites through time within the Shikoku Basin. Notably, modern turbidites are not able to extend much further than the trench (Ike et al., 2008). However, uplift of the Shikoku basin initiated in late Miocene to early Pliocene, before the Nankai trough was well developed, allowed turbidite deposition far into the Shikoku Basin (Karig, 1975). Turbidity current deposits at Site 297 are discussed as occurring at depths ranging from 330-570 mbsf (Pickering et al., 1993). Base on nanofossil age constraints the turbidites predate the Pleistocene-Pliocene boundary of ~2.6 Ma at 210 mbsf and are above middle to late Miocene sediment (~11.6-16 Ma) at 630 mbsf. Sediment contained within the depth range of observed turbidites is early Pliocene in age (~3.6-5.3 Ma) at 350-440 mbsf (Shipboard Scientific Party, 1975). Using sediment accumulation rates from Site 1177 (nearest age corollary core) an age of ~3.20 Ma was determined for sample 297-12. Using the same sediment accumulation rates as sample 297-12 ages for the top and bottom of observed turbidites were determined. The base of the turbidite succession at 570 mbsf is ~11.8ma and is ~5.2 Ma at the top (330 mbsf). This suggests that the turbidite contained within sample 297-12 is ~2 Ma younger than the earliest observed turbidite at Site 297, and that turbidite deposition at Site 297 occurred over a longer period of time than previously thought.

The high clay content and fine grain size, coupled with glass chemistry indicative of multiple magmatic sources are most consistent with sediment from sample 297-12 being the distal part of a turbidite (Bouma sequence E). The development of the Nankai Trough coinciding with the last observed turbidite (330 mbsf) supports the lack of coarser

Bouma sequences A through D within sample 297-12. Many workers have demonstrated the affect topography has on sediment transport for turbidity currents and its ability to restrict all but the finest grain portion of the turbidite (Bouma Sequence E) being carried beyond the obstruction (i.e. Nankai Trough) (Alexander and Morris, 1994; Kneller and McCaffrey, 1999). This turbidite containing glass from multiple magmatic sources was most likely initiated through slope instability on the shelf where sediment from multiple volcanic sources accumulated (Schneider et al., 2001). Sedimentary structures, glass morphology and other petrographic features of sample 297-12 are similar to the other clay-dominated samples with ~2-13% disseminated glass. Thus, the chemical analyses of volcanic glass in sample 297-12 are critical for indicating the reworked sediment includes material from multiple magmatic events.

1.5.3 Glass Alteration

Clay content, shard morphology and chemical composition differ greatly between the rhyolitic glass within samples 442-28 and 444-16. Although sample 442-28 is not a discrete ash layer (~91% clay minerals, ~2% volcanic glass) it exhibits many of the characteristics typical of a single-sourced, explosive rhyolite (Perkins et al., 1995). These features include a tight grouping in glass composition (Figs. 1.4, 1.5, and 1.6). In contrast, the wide range in glass composition of SiO_2, K_2O, Na_2O and a tight grouping of FeO and CaO for the sample 444-16 ash layer (~95% volcanic glass) suggests either: 1) simultaneous ash deposition from multiple magmatic sources with distinct glass chemistry, 2) deposition from eruptions at one source with fractional crystallization within a single magma chamber (Schneider et al., 2001), or 3) diagenetic alteration of glass from a single source.

The chemical composition of sample 444-16 likely reflects alteration due to glass interacting with sediment pore water. As alkali elements are extremely mobile (i.e. easily leached from volcanic glasses), and FeO and CaO in glass are not greatly affected by alteration due to the interaction with seawater, their concentrations in the sample 444-16 support alkali element mobility through increased water-rock interaction. Silica within volcanic glass has also been shown to be highly mobile under advanced alteration processes (White et al., 2009) and this mobility may explain the wide range in SiO_2 concentrations. The ash layer of sample 444-16 is most likely not the result of simultaneous glass deposition from two or more sources or fractional crystallization within the magma chamber during eruption. An ash layer having two volcanic sources should exhibit a bimodal distribution of element compositions, which is not observed for sample 444-16 (Fig. 1.4). Also the tight grouping of FeO and CaO (Fig. 1.5) for the majority of glass analyses suggests sample 444-16 is sourced from a single magmatic event. Fractional crystallization during a single eruptive event could account for the variability in Si and alkali elements. As magma chambers evolve the composition of the melt becomes more rhyolitic, causing enriched in SiO_2, Na_2O, K_2O, and depletion in MgO, FeO, and CaO (Hildreth, 1981; Sigurdsson, 2000). Also, elements in a zoned magma chamber tend to covary in a linear fashion, rather than exhibiting wide, uncorrelated compositional variation. While sample 444-16 does exhibit differences in SiO_2, Na_2O, and K_2O the lack of correlation between these elements, as well as the lack of variability in FeO and CaO (Fig. 1.5) rules out fractional crystallization as a cause for the unique chemical signature of the ash layer.

Differences in the degree of glass alteration between the 442-28 and 444-16 rhyolite glass shards can be caused by differing thermal histories, different amounts of water-rock interaction, or differences in the susceptibility of the shards to alteration (i.e. differences in size and/or morphology) (Hajash and Chandler, 1981). Greater alteration of the 444-16 glass shards may result from: 1) a warmer thermal history, 2) longer time for alteration, 3) greater volume of pore fluid cycling through the system, or 4) shards more physically susceptible to alteration (i.e. greater surface area/volume). We explore the potential differences between the thermal histories for each sample. For all samples except 297-12 the thermal histories are very similar (Fig. 1.8). Both 442-28 and 444-16 are ~12 Ma. The modeled thermal histories predict a maximum difference in temperature of 7 ˚C (higher for the 444-16 sediment) at 7 Ma after deposition. More rapid heating of the 442-28 sediment in the intervening ~5 Ma shifts it to slightly higher temperatures than the 444-16 sediment. These small (and compensating) differences in thermal history would produce little difference in kinetically-driven glass alteration progress between the two

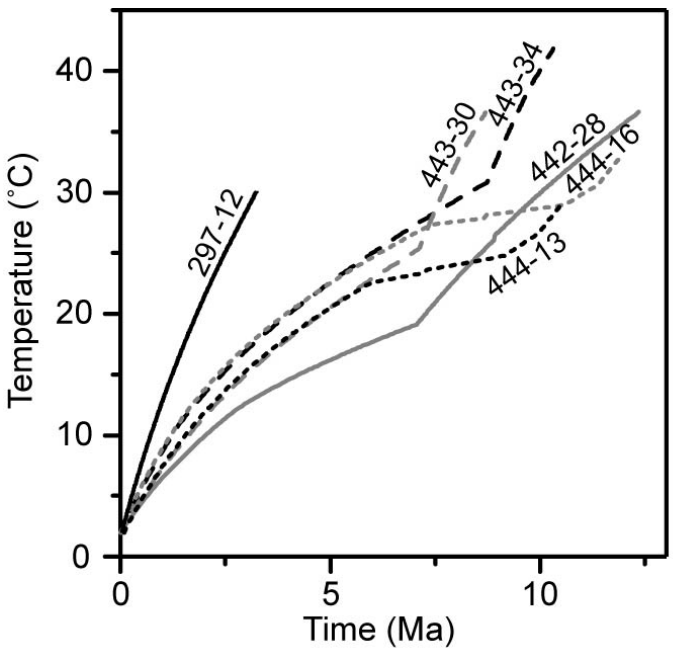

Figure 1.8: Thermal history for our sediment samples based on sediment accumulation rates and 1-D transient heat conduction. All samples excluding 297-12 have very similar thermal histories.

samples. This suggests that the differences in glass alteration between samples 442-28 and 444-16 are not driven by a longer or warmer thermal history for the 444-16 sediment.

Sample 444-16 is an ash layer with much lower clay content than the five other samples. Ash layers commonly have high porosity (Tribble and Wilkens, 1994) and higher permeability than surrounding clay-dominated sediment (Saffer et al., 2000). A high permeability ash layer likely experienced much more fluid flow than the surrounding hemipelagic sediment. Thus, glass shards within the ash layer may have experienced more water-rock interaction than shards disseminated throughout the hemipelagic sediment. Laboratory experiments on glass alteration for samples with the same thermal history indicate that rhyolitic glass subject to higher water-rock ratio leach more alkali elements (Hajash and Chandler, 1981). This scenario explains the broad distribution in total alkali content for the 444-16 glass. The element SiO_2 is also variable between glass shards in sample 444-16. SiO2 is typically considered to be a more immobile element during the glass alteration process (Stefansson and Gislason, 2001; Gislason, 2008), although in some studies, SiO2 has been shown to be mobile (Berger et al., 1987; White et al., Submitted). Furthermore, at ODP Sites 1173 and 1177 (in the Shikoku Basin, landward of Site 297) significant alteration of discrete ash layers and disseminated amorphous silica occurs at the same depth (Spinelli et al., 2007), suggesting that SiO_2 is mobile during the glass alteration process in this environment. Samples from Sites 442, 443, and 444 (in the Shikoku Basin seaward of Site 297) show little evidence of glass alteration where amorphous silica concentrations similar to Sites 1173, 1177, and 297 are found. This difference in glass dissolution suggests the thermal history is the primary control on glass alteration progress both in ash layers and in the hemipelagic

sediment. The difference in glass alteration mechanisms between sites (1173 and 1177) and (442, 443, and 444) may result from different sediment accumulation rates. The Site 1173 and 1177 sediments were buried quickly causing a rapid increase in temperature. Approximately 5 Ma after deposition, sediment at Sites 1173 and 1177 were exposed to temperatures >50^{o}C; the same age sediment at Site 444 is at ~22^{o}C. This suggests that the amount of glass alteration within sediment that warms very slowly (i.e. slow sediment accumulation, far from the trench is sensitive to the water-rock ratio. In rapidly heated sediments (i.e. rapid burial, close to trench), thermal history is the primary control on glass alteration (i.e. rapid heating overwhelms differences in water-rock interaction).

1.6 CONCLUSIONS

Volcanic glass in Shikoku Basin sediments is derived from the Izu-Bonin arc (basaltic andesite) and the Japanese arc (explosive rhyolitic eruptions). Glasses in sample 444-16 have unusually high FeO content for a rhyolitic eruption. The only source within the region known to produce glass with similar composition is Baegdusan volcano on the border of North Korea and China. Though, the sample 444-16 ash layer pre-dates known activity from Baegdusan an older volcano within the same region may produce glass with similar high FeO content that is transported to Site 444 within the Shikoku Basin through a 60^{o} shift in wind direction. Due to its unique chemistry, the sample 444-16 ash layer is well suited as a stratigraphic marker that may allow intercorrelation between different sediment cores. In addition, identification of an appropriate aged volcanic source would lead to greater insight into the complexities of ash distribution around the Japanese islands.

Though the exact sources of volcanic material contained within sample 297-12 were not determined, glass chemistry data clearly indicate that this sample contains material from multiple magmatic events and sources. The fine grain size and high clay content coupled with glass compositions that show a large variability in relatively immobile elements and a small range in mobile elements indicate sample 297-12 is a distal turbidite. Sample 444-16 represents a discrete ash layer from a single magmatic source that has undergone extensive alteration post deposition due to sea water interaction. The high permeability (low clay content and large grain size) ash layer allowed extensive water-rock interaction leading to significant alteration causing a wide spread in mobile alkali elements (Na_2O and K_2O) as well as Si which has been shown to mobilize during advanced glass alteration. Sample 444-16 compared to other high clay content samples demonstrates the ability of clay to lower water-rock interaction and affect element mobility.

Glass geochemical analyses are commonly used to identify potential volcanic sources.

However, in these Shikoku Basin samples, glass chemistry also provides information on sedimentological and diagenetic processes. The five samples examined comprising clay-dominated sediments with disseminated glass do not visibly (macroscopically or microscopically) display clear sedimentological differences. Yet, the glass chemistry data clearly indicate that sample 297-12 is a turbidite, and the others are consistent with hemipelagic sediment accumulation. In fine grained marine sediments, such as these, in which macroscopic textural variation is minimal, and sedimentary structures are largely

lacking, quantitative analysis of glass chemistry can be an extremely valuable tool for interpreting both depositional and diagenetic processes affecting the sediments.

CHAPTER 2: GLASS ALTERATION AND SEDIMENT CEMENTATION

2.1 INTRODUCTION

A small amount of cement can strengthen sedimentary rocks and affect their deformation (Clough et al., 1981; Karig, 1993; Schnaid et al., 2001; Saidi et al., 2003; Spinelli et al., 2007). In marine environments, quartz, calcite, authigenic clay minerals, and zeolite commonly act as cements (Larsen, 1983). Volcanic glass is a potentially important, though little investigated, source of cement in marine sediments; glass alteration products (e.g., palagonite, allophone, and saponite) have been shown to increase sediment strength (Schiffman et al., 2006). In marine sediments, volcanic glass is either present as discrete ash layers or is dispersed throughout the sediment column. For example, in the Shikoku Basin offshore the Japanese volcanic arc, the dominantly hemipelagic sediment is punctuated by multiple ash layers (Shipboard Scientific Party 2001). However disseminated glass dispersed throughout the sediment column in many cases have been shown to be in greater volume than glass contained within discrete ash layers (Huang, 1980). This disseminated glass may play an important role in cementation of sediment due to its presence throughout the sediment column. Though the disseminated glass represents only a small fraction of the total sediment, as little as 1-2 wt% cement can dramatically strengthen sediment (Clough et al., 1981; Schnaid et al., 2001). The process of glass alteration and the minerals these processes form have been extensively studied for basaltic glass (Crovisier et al., 1983; Zhou et al., 2001) and to a lesser extent for rhyolitic glass (Hajash and Chandler, 1981). Many glass alteration

products demonstrate diagnostic major element enrichment or depletion relative to their source glass. This chemical alteration may be used for identification, as well as aiding in the understanding of the processes that led to their formation.

Previous work on Shikoku Basin sediment identified a Si-rich amorphous phase coating grains. The coating occurs in zones with high amorphous silica content and elevated (nearly constant) porosity within the upper Shikoku Basin facies at Ocean Drilling Program (ODP) Sites 1173 and 1177 (Spinelli et al., 2007). Sharp physical and chemical changes that mark the base of this cemented zone are used to define a diagenetic boundary separating upper Shikoku Basin facies from lower Shikoku Basin facies sediment (Shipboard Scientific Party, 1991; 2001). Here we examine six additional sites within Shikoku Basin (Deep Sea Drilling Project (DSDP) Sites 297, 442, 443, and 444, and Integrated Ocean Drilling Program Sites C0006 and C0007) to determine the extent and source of the cement.

2.2 SITE DESCRIPTION

2.2.1 Site 297

Site 297 is ~100 km seaward of the Nankai Trough subduction zone on ~23 Ma crust (Fig. 2.1). The estimated total sediment thickness is 780 m; 680 m were drilled on DSDP Leg 31 (Shipboard Scientific Party, 1975). The sediments are primarily hemipelagic mud with ash, silt, and sand interbeds (Fig. 2.2; Shipboard Scientific Party, 1975). The upper/lower Shikoku Basin facies boundary at Site 291 has been defined based on age relations (Fox, 1996) rather than as a diagenetic boundary as at Sites 808, 1173, 1174, and 1177 (Shipboard Scientific Party, 1991; 2001). The upper Shikoku Basin facies and upper portion of the lower Shikoku Basin facies sediment have high and

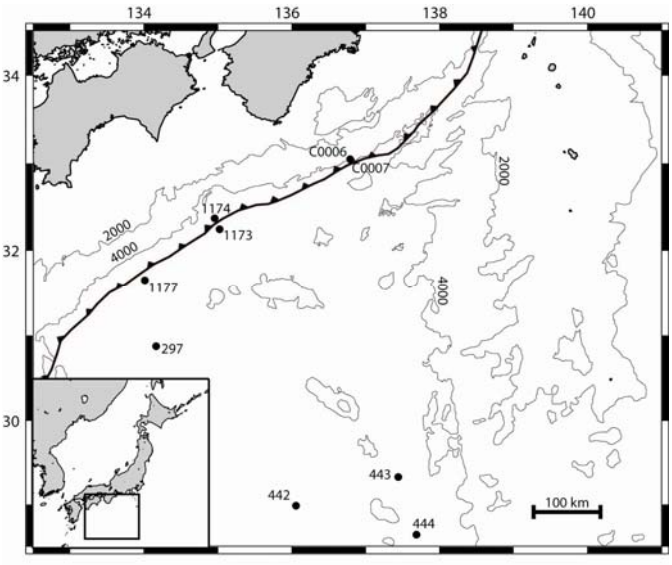

Figure 2.1: Location of DSDP Sites 297, 442, 443, 444, ODP Sites 1173, 1174 and 1177, and IODP Site C0006 and C0007 in the Shikoku Basin. Thin lines are bathymetry in meters. Barbed line is Nankai Trough subduction zone deformation front.

nearly constant porosity (Fig. 2.3). A step drop in porosity occurs ~350 meters below seafloor (mbsf) within the lower Shikoku Basin facies. We examine sediment samples throughout the upper Shikoku Basin and lower Shikoku Basin facies; the sediment is dominantly (~85%) clay minerals with ~3% volcanic glass (Shipboard Scientific Party, 1975).

2.2.2 Sites 442, 443, 444

Sites 442, 443, and 444 are approximately 400 km from the trench on slightly younger crust than Site 297; they are closer to the fossil spreading ridge (Fig. 2.1). Sediment at Sites 442 and 444 is ~410 m thick; at Site 443 there is ~580 m of sediment (Shipboard Scientific Party, 1980a; 1980b, 1980c). At all three sites, the sediment consists of hemipelagic mud with some distinct ash layers and some disseminated ash; ~60-95% clay and ~2-13% volcanic glass (Shipboard Scientific Party, 1980a, 1980b, 1980c). Similar to Site 297, the upper/lower Shikoku Basin facies boundary is defined based on age relations, not diagenetic reaction progress We examine sediment samples

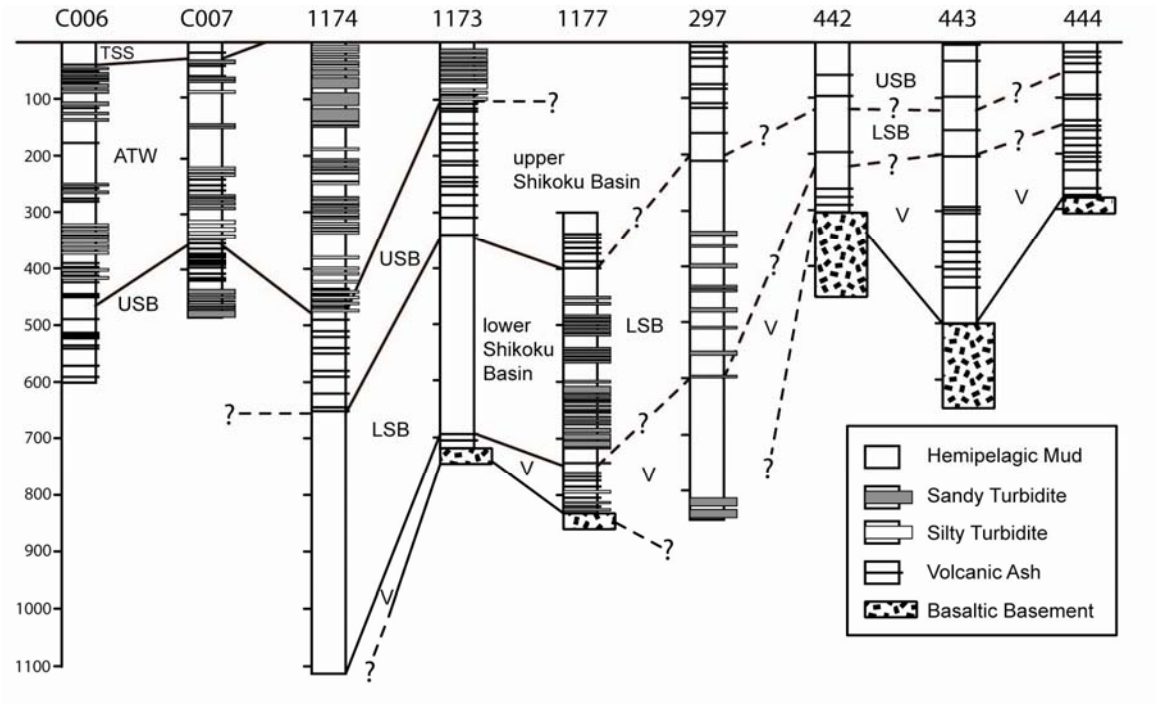

Figure 2.2: Stratigraphic correlations between drill sites in Shikoku Basin and on the Nankai margin (Klein and Kobayashi, 1981; Shipboard Scientific Party, 2001; Shipboard Scientific Party, 2008). TSS= trench slope sediment; ATW= axial trench wedge; USB= upper Shikoku Basin facies; LSB= lower Shikoku Basin facies; V= volcaniclastic

from the upper Shikoku Basin facies, lower Shikoku Basin facies, and the section below the lower Shikoku Basin facies.

2.2.3 Site C0006 and C0007

Sites C0006 and C0007 are landward of the trench (Fig. 2.1) and were designed to sample the main frontal thrust of the accretionary wedge (Shipboard Scientific Party, 2008). Sediments at Sites C0006 and C0007 comprise upper Shikoku Basin facies sediment overlain by trench wedge sediment and a drape of slope sediment (Shipboard Scientific Party, 2008). We examine sediment samples from the trench wedge and upper

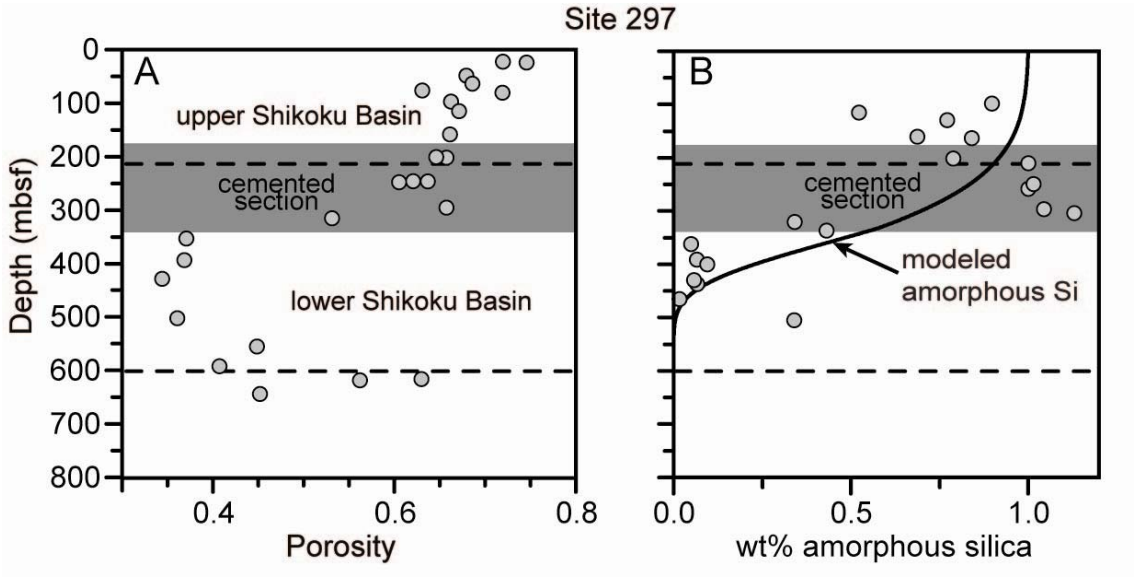

Figure 2.3: Site 297 sediment porosity (A; Shipboard Scientific Party, 1975) and amorphous Si content (B). Dashed lines are inferred lithologic boundaries (Klein and Kobayashi, 1981). Solid line is modeled amorphous Si content based on sediment thermal history and amorphous Si reaction kinetics. Gray band is predicted location of cemented section based on amorphous Si alteration. The base of the cemented section coincides with a steep drop in both porosity and amorphous Si.

Shikoku Basin facies at Site C0006 and one sample from the upper Shikoku Basin facies at C0007.

2.4 METHODS

2.4.1 Amorphous Silica Content

Amorphous silica content of bulk sediment samples was measured using an alkaline leaching method (DeMaster, 1981). Approximately 100 mg of freeze-dried sediment was digested in 40 mL of 1.0 wt% $NaCO_3$ (pH = 11.4) at 85 ^oC. A pH 11.4 solution was used to minimize clay mineral digestion (Schluter and Rickert, 1998). Once the digestion process began, 0.200 mL aliquots of leachate were taken at 5, 15, 30, 60, 90, 120, 200, and 300 minute intervals. Silica concentration in the leachate (determined by spectrophotometry; Grassholf et al., 1983) increases as both amorphous silica (e.g.,

glass, opal) and structured silicates (e.g., clay, quartz, feldspar) in the sediment dissolve. The amorphous silica dissolves quickly, dominantly controlling silica content in the leachate early; the contribution of dissolved silica from structured silicates is slower and more prolonged. A break in slope in leachate silica content versus time indicates exhaustion of amorphous silica sources, allowing calculation of the amorphous silica content of the sediment (DeMaster, 1981). For each sediment column examined, we simulate sediment accumulation and 1-D heat conduction. We use the modeled thermal history for the sediments to estimate the amount of dissolution of amorphous silica (e.g., Spinelli et al., 2007).

2.4.2 Petrographic Analysis

Samples were examined using backscattered electron (BSE) imaging on a Cameca SX-100 microprobe at New Mexico Tech. Operating conditions for the microprobe were 15kV acceleration voltage and 20 nA beam current. Vacuum and surface impregnation techniques were used in order to preserve the texture and structure of the samples during lapping and polishing. Slides were polished, evaporatively coated with carbon, and analyzed using quantitative elemental analysis of selected phases using wavelength-dispersive spectrometer (WDS) scans (Reed, 1996). Most analyses were conducted using a beam diameter of 10 μm, due to the small size of the material of interest; where possible a 15 or 20 μm beam was used. Analysis points were quantitatively analyzed to determine the percentage of Si, Al, Ti, Fe, Mn, Mg, S, Ca, Cl, Na, and K. Standard reference samples of feldspars, amphiboles, and glasses were analyzed at the beginning and end of each analytical run in order to be able to calculate analytical accuracy and precision, as well as to monitor instrument calibration.

Additional samples with minimal preparation (i.e. volume of sediment broken open and fresh surface sputter coated with carbon) were analyzed by secondary electron imaging (SEM) under low vacuum on the JEOL 5800LV at the University of New Mexico. Weight percentages of elements Si, Al, Ti, Fe, Mg, Ca, Cl, Na, and K were measured using electron dispersive scans (EDS). An accelerating voltage of 20 kV and a live time of 75 seconds were used.

2.5 RESULTS

We use the measured amorphous Si content of bulk sediment samples to define potential diagenetic boundaries and examine possible relationships between amorphous Si content and porosity (e.g., Spinelli et al., 2007). BSE and SEM image analyses are used to determine the source of amorphous Si and controls on the formation of this material. For most of the sites, samples analyzed cover the stratigraphic intervals of the upper and lower Shikoku Basin facies; samples from Sites C006 and C007 are from the upper Shikoku Basin facies and overlying trench wedge sediment.

2.5.1 Measured Amorphous Si Content

At Site 297, sediment above 350 mbsf contains ~0.5-1.0 wt% amorphous silica (Fig. 2.3). From 305 to 356 mbsf, amorphous silica content drops from ~1 wt% to <0.1 wt%. Sites 442, 443, and 444 have relatively high Si content (~1-2.5 wt%) throughout the entire sediment column (Fig. 2.4). These three sites lack the marked drop in Si content observed at Sites 297 (Fig. 2.3), 1173, 1174, and 1177 (Spinelli et al., 2007). At Sites C006 and C007, sediment above and within the upper Shikoku Basin facies contains ~1 wt% amorphous silica (Fig. 2.5).

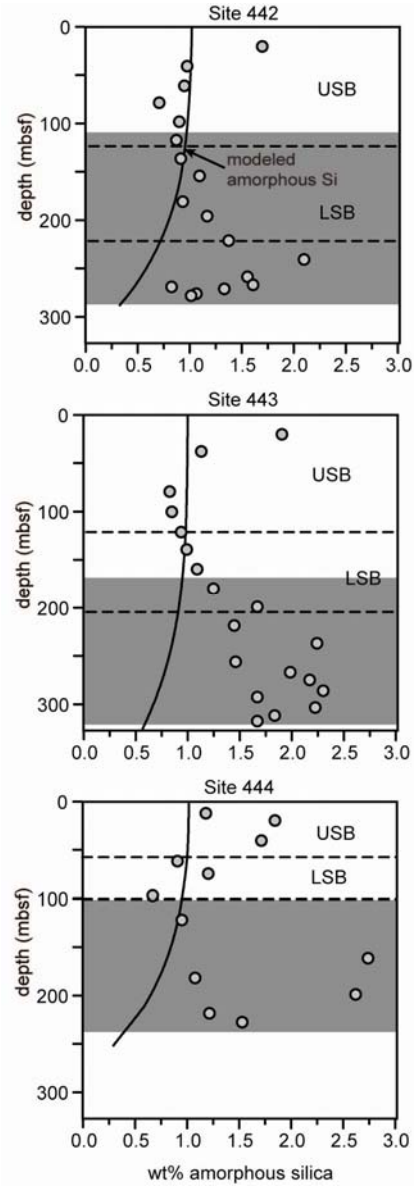

Figure 2.4: Amorphous Si content of sediment at Sites 442, 443, and 444. Dashed lines are inferred lithologic boundaries (Klein and Kobayashi, 1981). Solid line is modeled amorphous Si content. Gray band is modeled cemented section. The cemented section has >1 wt% amorphous Si; the base of the cemented section is not observed at these sites.

2.5.2 Image Analysis

Based on BSE and SEM image analyses, all sites examined contain abundant disseminated volcanic glass fragments. These volcanic glass fragments ranged in physical condition from pristine, angular, and unaltered to pitted, highly dissolved and weathered (Fig. 2.6, 2.8). Glass pieces and surrounding material were analyzed using wavelength-dispersive spectrometer (WDS) scans and electron dispersive (EDS) scans. Our investigation focuses on Site 297, where the trend in amorphous silica content versus depth is similar to those for Sites 1173, 1174, and 1177.

Sample 297-12 (249 mbsf) is representative of sediment analyzed from a zone with high porosity and high amorphous silica content (Fig. 2.3). The bulk sediment is dominantly clay. The BSE image in Figure 2.6 shows a large feldspar grain encased by a rim of partially altered volcanic glass, within the clay matrix. Four points in this field (A, B, C, and

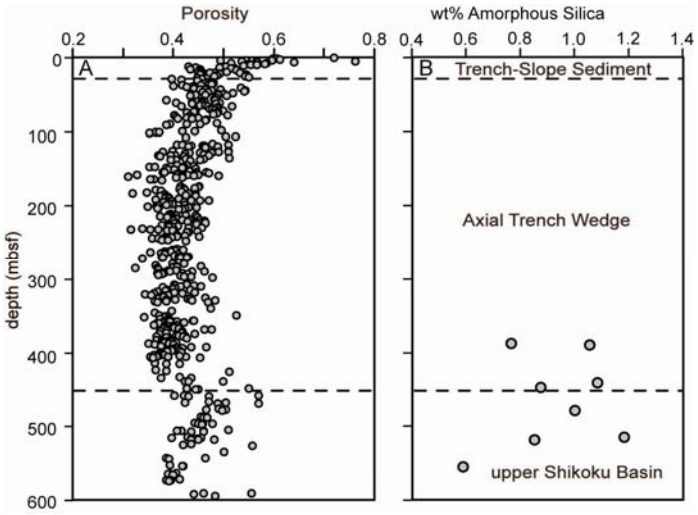

Figure 2.5: Site C0006 sediment porosity (A; Shipboard Scientific Party, 2008) and amorphous Si content (B). Dashed lines are facies boundaries (Shipboard Scientific Party, 2008).

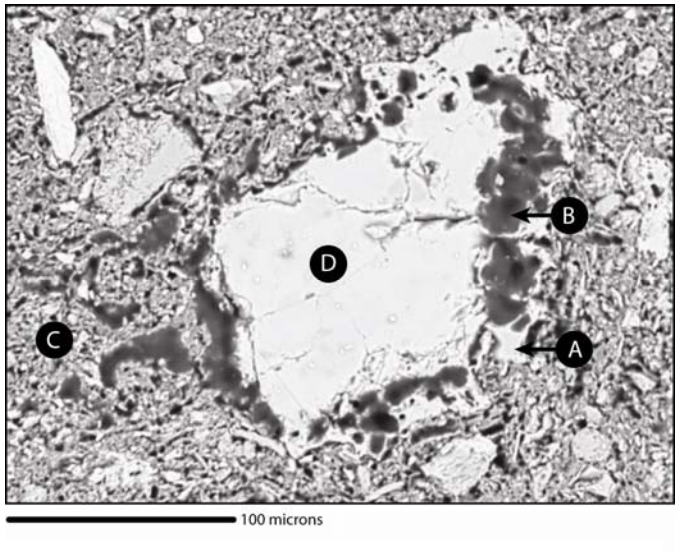

Figure 2.6: Representative backscattered electron (BSE) image of highly altered glass (A) with amorphous Si-rich material filling pore space (B). The sediment is dominantly clay matrix (C). Point D and surrounding bright area is a feldspar grain that is encased in volcanic glass (A).

D) were quantitatively analyzed to determine their major element compositions. The composition at point D is consistent with feldspar. Chemical composition at point A indicates a hydrated (analytical total of ~90 wt.%) dacitic glass (Fig. 2.7). The amorphous (and low mean atomic number) material around the volcanic glass and filling surrounding pore space was analyzed at point B. This material has significantly lower totals (~20 wt%) than the volcanic glass, but has similar major element ratios. The compositional distribution of the glass, scaled to the low total for the alteration product, is indicated by horizontal black lines in the Figure 2.7. This represents the wt% of each element had the alteration

product (B) only been affected by the lower total (i.e. only loss of material/hydration, no change in composition). Measured elemental wt% below the line indicates depletion; measured values above the line indicate enrichment. The alteration product is slightly depleted in Si, Al, and Ca, with a larger depletion in Na. Magnesium is appreciably enriched; iron is slightly enriched.

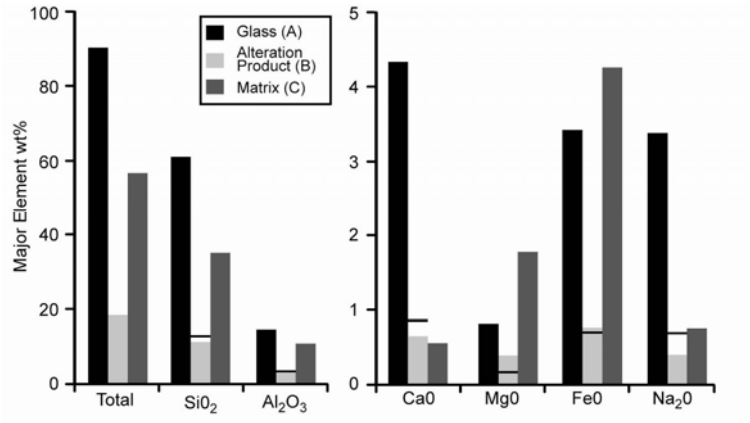

Figure 2.7: Results of un-normalized BSE chemical analysis corresponding to points A, B, and C for sample 297-12 (Fig. 6). Analysis point A is typical of hydrated andesitic volcanic glass with ~90 wt% analytical totals and ~60 wt% Si. Point B has much lower analytical totals relative to the glass (A) suggesting a large volume of material has migrated away from the site of alteration. Black horizontal lines indicate composition of alteration product had it only been affected by a lower total caused by a loss of material. Analysis of the matrix (C) is consistent with detrital smectite.

Glass shards from sample 297-12 also were analyzed quantitatively using SEM. Similar to samples analyzed on prepared microprobe polished thin sections, an amorphous material was found in the proximity of volcanic glass contained within the minimally prepared SEM analyzed samples (Fig. 2.8). The amorphous material coats clay particles. Both the volcanic glass (A) and the amorphous material (B) (Fig. 2.9) are similar in composition to glass and amorphous material analyzed using BSE image analysis (Figs. 2.6, 2.7). The amorphous material is depleted in Si, Ca and Na, and is enriched in Mg and Fe. Aluminum shows enrichment of < 1wt%.

Sediment samples from Sites 442, 443, 444, and C006 were also analyzed using both BSE and SEM images analysis. We found abundant disseminated glass throughout the sediment column. The glass contained within these samples ranged in physical condition from pristine fresh glass to pitted and weathered, similar to Site 297. However, the amorphous material associated with glass from within the cemented section at Site 297 was not observed at these sites.

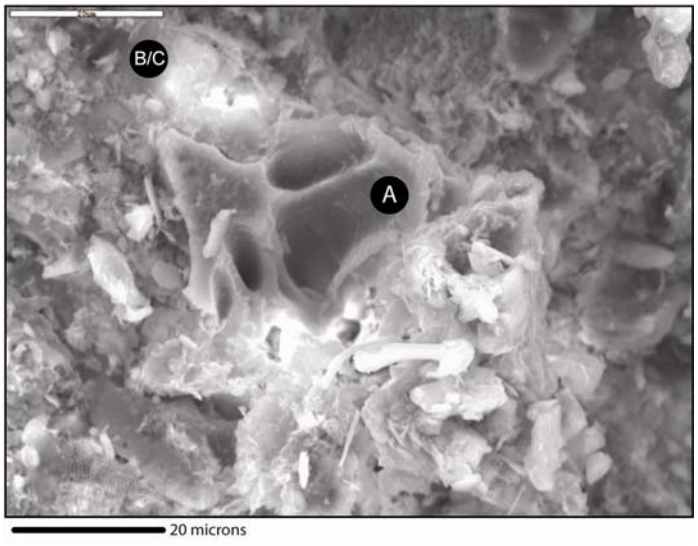

Figure 2.8: Representative secondary electron microscopy (SEM) image of altered glass shard (A) with amorphous Si-rich material (B) coating clay grains (C) from sample 297-12.

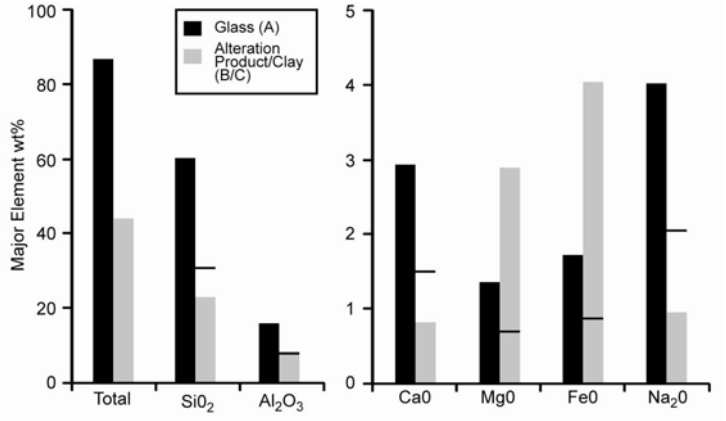

Figure 2.9: Results of un-normalized BSE chemical analysis corresponding to points A and B for sample 297-12 (Fig. 9). Analysis point A is typical of hydrated andesitic volcanic glass with ~87 wt% analytical totals and ~60 wt% Si. Similar to BSE analysis (Fig. 7) point B also has lower analytical totals relative to the glass (A) suggesting a large volume of material has migrated away from the site of alteration. Black horizontal lines indicate composition of alteration product had it only been affected by a lower total caused by a loss of material.

2.6 DISCUSSION

2.6.1 Measured Amorphous Si

At Site 297, the sediment from ~100-350 mbsf has high (and nearly constant) porosity and high amorphous silica content. At the base of this zone,

amorphous silica content and porosity both drop abruptly. This is indicative of a zone of cemented sediment from ~100-350 mbsf comparable to those ~100-200 km north at Sites 1173 and 1177 (Spinelli et al., 2007). To be consistent with the lithologic descriptions at Sites 808, 1173, and 1177, the upper Shikoku Basin/lower Shikoku Basin facies boundary at Site 297 should be defined at ~350 mbsf, approximately 175 m deeper than the demarcation based on age relations. Site 442, 443, and 444 sediments also have high amorphous Si content within a zone with temperatures similar to the cemented zones at Sites 297, 1173, and 1177. Thus, these Site 442, 443, and 444 sediments may be cemented by the same process and these sections likely are equivalent to the upper Shikoku Basin facies. These sites lack the transition from high to low amorphous silica content with increasing depth (i.e. the upper/lower Shikoku Basin facies boundary likely is below the sediments examined). This likely is due to the thinner sediment column at Sites 442, 443, and 444. The basal sediments at these sites may be heated sufficiently for diagenetic cementation to have begun, but additional heating and breakdown of the cement has not occurred yet. As the sediment at these sites is buried further, the diagenetic boundary separating high amorphous silica content cemented sediment and low amorphous silica content uncemented sediment may develop. In the accretionary prism, at Sites C006 and C007, trench wedge and upper Shikoku Basin sediment have amorphous silica concentrations (~1 wt%) similar to the cemented section in the Shikoku Basin sites (Fig. 2.5).

2.6.2 Source of Cement

The cemented zones at Sites 1173 and 1177 have been proposed to result from opal (sourced from siliceous tests) diagenesis (Spinelli et al., 2007). This hypothesis fits

the cemented section's ability to preserve porosity evenly across the entire cemented section. Siliceous tests that settle to the ocean floor would be distributed evenly throughout the hemipelagic Shikoku Basin sediment section allowing for homogeneous distribution of the associated amorphous silica. In addition, preliminary BSE and SEM analyses of the cementing material were consistent with opal (i.e. amorphous; primarily Si and Al). Further study indicates volcanic glass is likely the source of an amorphous Si-rich gel cementing upper Shikoku Basin sediment. Abundant disseminated glass was observed at Sites 297, 442, 443, 444, and C006. Disseminated glass at Site 297 is partially altered to an amorphous material with abundant Si and Al. Proximity and similarity in chemical composition suggest that the amorphous silica-rich gel is derived from glass alteration.

2.6.3 Glass Alteration

Most studies of volcanic glass alteration and glass alteration products focus on basaltic glass. We use these basalt-focused studies as an analog for processes occurring within the basaltic andesite to rhyolitic glass found within sample 297-12 at Site 297. The amorphous Si gel associated with the disseminated volcanic glass of sample 297-12 is depleted in Si, Al, Ca, and Na; it is enriched in Mg and Fe. These chemical trends are consistent with amorphous silica gels sourced from basaltic glass that later form crystalline clays (Berger et al., 1987). However, there are critical differences between the chemistry of alteration products associated with basaltic glass (Berger et al., 1987; Zhou et al., 2001) and the amorphous material we analyzed. Basaltic glass alteration products commonly have ~85-90% analytical totals (Berger et al., 1987; Zhou et al., 2001) suggesting a 10-15% loss in material/hydration. The alteration product in the Site

297-12 sample has analytical totals of ~44 wt% (SEM chemical analysis) to ~18% (electron microprobe chemical analysis), indicating larger loss in material. These differences in analytical totals may be explained by varying degrees of glass alteration. The glass in the BSE image (Fig. 2.6) appears to be highly dissolved and has the highest degree of alteration, while the glass in the SEM image (Fig. 2.8) is relatively fresh with sharp well defined edges. The basaltic glass analyzed in earlier studies (e.g., Berger et al., 1987; Zhou et al., 2001) may be even less dissolved, as indicated by the higher total wt% detected within the amorphous gel material.

As glass alteration progresses, more silicate gel is formed allowing greater amounts of material to move away from the glass and interact with the surrounding sediment. The alteration product is mobile, filtering out into pore space and coating clay far from the source glass (Fig. 2.6). Similar Si-rich amorphous material has been observed coating clay grains within the cemented section of Site 1173 (Spinelli et al., 2007).

We propose that the formation of volcanic-glass-derived, Si-rich amorphous gel is common throughout the Shikoku Basin. Volcanic glass disseminated through the hemipelagic sediment of Shikoku Basin is hydrated and heated upon burial and altered to a Si-rich gel. The gel with much lower density than its glass source spreads through the surrounding sediment, coating grains and cementing grain contacts (Fig. 2.10). With further burial and heating this intermediate glass alteration product is transformed to palagonite or authigenic clay that does not act as cement.

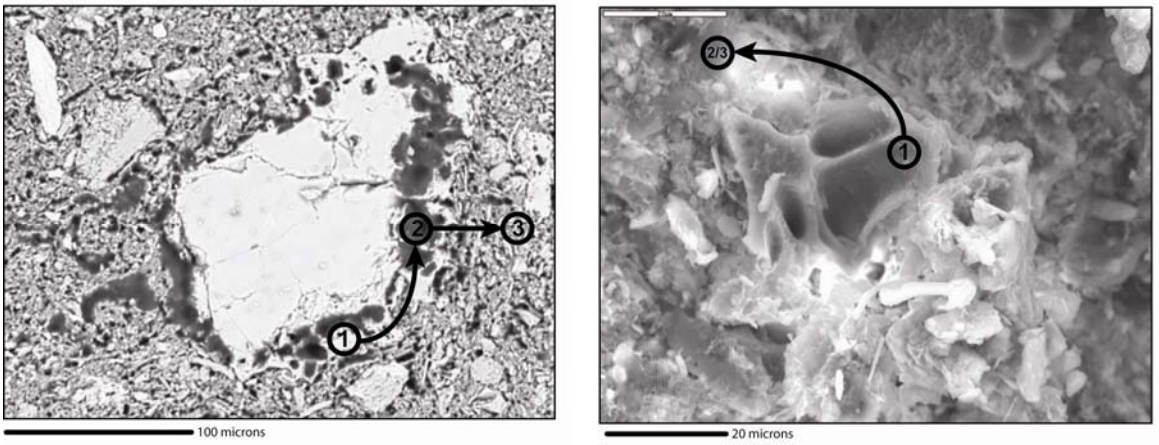

Figure 2.10: BSE (left) and SEM (right) images for sample 297-12 demonstrating the process of glass alteration (1) creating an amorphous Si rich material (2) that coats clay grains within the matirx (3) strengthening sediment and preserving porosity.

2.7 CONCLUSIONS

A minor amount of cement within marine environments can strengthen sediment and inhibit consolidation. Spinelli et al., (2007) provided evidence for ~1 wt% Si cement strengthening sediment and preserving porosity within Upper Shikoku Basin facies sediment at Sites 1173 and 1177 (Fig. 2.1). Additional analyses at Sites 297, 442, 443, 444, C0006 and C0007 indicate that cementation of sediments above a diagenetic boundary is common throughout the Shikoku Basin.

Through a combination of imaging and chemical analyses, we identify volcanic glass as the source of the Si cement that is strengthening the sediment. BSE imaging of the cemented zone show a Si-rich amorphous material near altered volcanic glass. Quantitative analysis of the glass and its alteration product show the two are similar in composition. However, the alteration product is slightly depleted in Si, Al, and Ca; it is enriched in Fe an Mg. This chemical signature is consistent with siliceous gel alteration products associated with glass pieces that have undergone extensive dissolution (Berger et al., 1987; Zhou et al., 2001). Here, we observe Si-rich amorphous material: 1) within

pore space created during glass dissolution, 2) filling pore space within the matrix, and 3) coating clay grains. These observations indicate that the glass alteration product is highly mobile and a small amount of glass is capable of cementing a large volume of sediment.

Throughout Shikoku Basin, volcanic-glass-sourced cement coats grains, strengthens sediment, and preserves porosity in the upper Shikoku Basin facies. Similar cementation may occur in other sedimentary basins where volcanic glass accumulates in the sediment and is heated and hydrated sufficiently to cause alteration. Heating of the sediment and alteration of the glass can occur at sites where the crust is relatively young and hot (e.g., Shikoku Basin; (Okino et al., 1994), and/or where sediment is deeply buried (i.e. thick) (e.g., Gulf of Alaska; (Brocher et al., 1994). In sedimentary basins this cementation affects sediment consolidation and porosity. In convergent margins, this strengthened sediment may affect deformation features as sediment is subducted or incorporated into the accretionary wedge.

REFERENCES

Alexander, J., and Morris, S., 1994, OBSERVATIONS ON EXPERIMENTAL, NONCHANNELIZED HIGH-CONCENTRATION TURBIDITY CURRENTS AND VARIATIONS IN DEPOSITS AROUND OBSTACLES: Journal of Sedimentary Research Section a-Sedimentary Petrology and Processes, v. 64, no. 4, p. 899-909.

Berger, G., Schott, J., and Loubet, M., 1987, FUNDAMENTAL PROCESSES CONTROLLING THE 1ST STAGE OF ALTERATION OF A BASALT GLASS BY SEAWATER - AN EXPERIMENTAL-STUDY BETWEEN 200-DEGREES-C AND 320-DEGREES-C: Earth and Planetary Science Letters, v. 84, no. 4, p. 431-445.

Brocher, T. M., Fuis, G. S., Fisher, M. A., Plafker, G., Moses, M. J., Taber, J. J., and Christensen, N. I., 1994, MAPPING THE MEGATHRUST BENEATH THE NORTHERN GULF OF ALASKA USING WIDE-ANGLE SEISMIC DATA: Journal of Geophysical Research-Solid Earth, v. 99, no. B6, p. 11663-11685.

Cerling, T. E., Brown, F. H., and Bowman, J. R., 1985, Low-temperature alteration of volcanic glass: hydration, Na, K, 18O and Ar mobility: Chemical geology, v. 52, no. 3-4, p. 281-293.

Clough, G. W., Sitar, N., Bachus, R. C., and Rad, N. S., 1981, CEMENTED SANDS UNDER STATIC LOADING: Journal of the Geotechnical Engineering Division-Asce, v. 107, no. 6, p. 799-817.

Crovisier, J. L., Thomassin, J. H., Juteau, T., Eberhart, J. P., Touray, J. C., and Baillif, P., 1983, EXPERIMENTAL SEAWATER BASALTIC GLASS INTERACTION AT 50-DEGREES-C - STUDY OF EARLY DEVELOPED PHASES BY ELECTRON-MICROSCOPY AND X-RAY PHOTOELECTRON SPECTROMETRY: Geochimica Et Cosmochimica Acta, v. 47, no. 3, p. 377-387.

Fox, P. J., 1996, Backarc basins. Tectonics and magmatism - Taylor,B: Science, v. 272, no. 5258, p. 381-405.

Furuta, T., and Arai, F., 1980, Petrographic and geochemical properties of tephras in deep sea drilling project cores from the North Philippine Sea: U.S. Govt. Printing Office.

Gislason, S. R., 2008, Weathering in Iceland: Jokull, v. 58, p. 387-408.

Haberle, S. G., and Lumley, S. H., 1998, Age and origin of tephras recorded in postglacial lake sediments to the west of the southern Andes, 44 degrees S to 47 degrees S: Journal of Volcanology and Geothermal Research, v. 84, no. 3-4, p. 239-256.

Hajash, A., and Chandler, G. W., 1981, An experimental investigation of high-temperature interactions between seawater and rhyolite, andesite, basalt and peridotite Contributions to Minerology and Petrology, v. 78, no. 3, p. 240-254.

Hildreth, W., 1981, GRADIENTS IN SILICIC MAGMA CHAMBERS - IMPLICATIONS FOR LITHOSPHERIC MAGMATISM: Journal of Geophysical Research, v. 86, no. NB11, p. 153-192.

Huang, T. C., 1980, A volcanic sedimentation model: Implications of processes and responses of deep-sea ashes: Marine Geology, v. 38, no. 1-3, p. 103-122.

Ike, T., Moore, G. F., Kuramoto, S., Park, J. O., Kaneda, Y., and Taira, A., 2008, Tectonics and sedimentation around Kashinosaki Knoll: A subducting basement high in the eastern Nankai Trough: Island Arc, v. 17, no. 3, p. 358-375.

Karig, D. E., 1975, Basin Genesis in the Philippine Sea, Initial reports of the Deep Sea Drilling Project: Washington D.C., p. 857-878.

Katoh, S., Nagaoka, S., WoldeGabriel, G., Renne, P., Snow, M. G., Beyene, Y., and Suwa, G., 2000, Chronostratigraphy and correlation of the Plio-Pleistocene tephra layers of the Konso Formation, southern Main Ethiopian Rift, Ethiopia: Quaternary Science Reviews, v. 19, no. 13, p. 1305-1317.

Kneller, B., and McCaffrey, W., 1999, Depositional effects of flow nonuniformity and stratification within turbidity currents approaching a bounding slope: Deflection, reflection, and facies variation: Journal of Sedimentary Research, v. 69, no. 5, p. 980-991.

Larsen, G., 1983, EARLY DIAGENESIS - A THEORETICAL APPROACH - BERNER,RA: Earth-Science Reviews, v. 19, no. 2, p. 174-175.

Lee, I. T., and Ogawa, Y., 1998, Bottom-current deposits in the Miocene-Pliocene Misaki Formation, IZU forearc area, Japan: Island Arc, v. 7, no. 3, p. 315-329.

Machida, H., 1999, The stratigraphy, chronology and distribution of distal marker-tephras in and around Japan: Global and Planetary Change, v. 21, no. 1-3, p. 71-94.

Norin, E., Albatross, and Svenska, d., 1958, The sediments of the central Tyrrhenian Sea: Göteborg, Elanders boktr.

Ogawa, Y., 1998, Bottom-current deposits in the Miocene-Pliocene Misaki Formation, Izu forearc area, Japan, Island Arc, Blackwell Publishing Limited, p. 315-329.

Okino, K., Shimakawa, Y., and Nagaoka, S., 1994, EVOLUTION OF THE SHIKOKU BASIN: Journal of Geomagnetism and Geoelectricity, v. 46, no. 6, p. 463-479.

Perkins, M. E., Nash, W. P., Brown, F. H., and Fleck, R. J., 1995, FALLOUT TUFFS OF TRAPPER-CREEK, IDAHO - A RECORD OF MIOCENE EXPLOSIVE VOLCANISM IN THE SNAKE RIVER PLAIN VOLCANIC PROVINCE: Geological Society of America Bulletin, v. 107, no. 12, p. 1484-1506.

Pickering, K. T., Underwood, M. B., and Taira, A., 1993, 26. Stratigraphic Sunthesis of the DSDP-ODP Sites in the Shikoku Basin, Nankai Trough, and Accretionary Prism: Procedings of the Ocean Drilling Program, Scientific Results, v. 131, p. 313-330.

Pouclet, A., Fujioka, K., Charvet, J., and Cadet, J.-P., 1986, Petrography and geochemistry of volcanic ash layers from Leg 87A, Nankai Trough (South Japan): U.S. Govt. Printing Office.

Reed, S. J. B., 1996, Electron Microprobe and Scanning Electron Microscopy in Geology, Cambridge University Press.

Saffer, D. M., Silver, E. A., Fisher, A. T., Tobin, H., and Moran, K., 2000, Inferred pore pressures at the Costa Rica subduction zone: implications for dewatering processes: Earth and Planetary Science Letters, v. 177, no. 3-4, p. 193-207.

Saidi, F., Bernabe, Y., and Reuschle, T., 2003, The mechanical behaviour of synthetic, poorly consolidated granular rock under uniaxial compression: Tectonophysics, v. 370, no. 1-4, p. 105-120.

Sarna-Wojcicki, A. M., Bowman, H. R., Meyer, C. E., Russell, P. C., Woodward, M. J., McCoy, G., Rowe, J. J., Jr., Baedecker, P. A., Asaro, F., and Michael, H., 1984, Chemical analyses, correlations, and ages of upper Pliocene and Pleistocene ash layers of east-central and Southern California: United States Geological Survey, Professional Paper, v. 1293, p. 40.

Scheidegger, K. F., Jezek, P. A., and Ninkovich, D., 1978, Chemical and optical studies of glass shards in Pleistocene and Pliocene ash layers from DSDP site 192, Northwest Pacific Ocean: Journal of Volcanology and Geothermal Research, v. 4, no. 1-2, p. 99-116.

Schiffman, P., Watters, R. J., Thompson, N., and Walton, A. W., 2006, Hyaloclastites and the slope stability of Hawaiian Volcanoes: Insights from the Hawaiian Scientific Drilling Project's 3-km drill core, p. 217-228.

Schnaid, F., Prietto, P. D. M., and Consoli, N. C., 2001, Characterization of cemented sand in triaxial compression: Journal of Geotechnical and Geoenvironmental Engineering, v. 127, no. 10, p. 857-868.

Schneider, J.-L., Le Ruyet, A., Chanier, F., Buret, C., Ferrière, J., Proust, J.-N., and Rosseel, J.-B., 2001, Primary or secondary distal volcaniclastic turbidites: how to make the distinction? An example from the Miocene of New Zealand (Mahia Peninsula, North Island): Sedimentary Geology, v. 145, no. 1-2, p. 1-22.

Self, S., Goff, F., Gardner, J. N., Wright, J. V., and Kite, W. M., 1986, EXPLOSIVE RHYOLITIC VOLCANISM IN THE JEMEZ MOUNTAINS - VENT LOCATIONS, CALDERA DEVELOPMENT AND RELATION TO REGIONAL STRUCTURE: Journal of Geophysical Research-Solid Earth and Planets, v. 91, no. B2, p. 1779-1798.

Shane, P. A. R., Black, T. M., Alloway, B. V., and Westgate, J. A., 1996, Early to middle Pleistocene tephrochronology of North Island, New Zealand: Implications for volcanism, tectonism, and paleoenvironments: Geological Society of America Bulletin, v. 108, no. 8, p. 915-925.

Shipboard Scientific Party, 1975, Site 297: Initial Reports of the Deep Sea Drilling Project, v. 31, p. 275-316.

Shipboard Scientific Party, 1980a, Site 442: Initial Reports of the Deep Sea Drilling Project, v. 58, p. 21-108.

Shipboard Scientific Party, 1980b, Site 443: Initial Reports of the Deep Sea Drilling Project, v. 58, p. 109-218.

Shipboard Scientific Party, 1980c, Site 444: Initial Reports of the Deep Sea Drilling Project, v. 58, p. 219-282.

Shipboard Scientific Party, 2001b, Site 1173: Procedings of the Ocean Drilling Program, Initial Reports, v. 190, p. 1-147.

Shipboard Scientific Party, 2001d, Site 1177: Procedings of the Ocean Drilling Program, Initial Reports, v. 190, p. 1-91.

Sigurdsson, H., 2000, Encyclopedia of Volcanoes.

Spinelli, G. A., Mozley, P. S., Tobin, H. J., Underwood, M. B., Hoffman, N. W., and Bellew, G. M., 2007, Diagenesis, sediment strength, and pore collapse in sediment approaching the Nankai Trough subduction zone: Geological Society of America Bulletin, v. 119, no. 3-4, p. 377-390.

Stefansson, A., and Gislason, S. R., 2001, Chemical weathering of basalts, Southwest Iceland: Effect of rock crystallinity and secondary minerals on chemical fluxes to the ocean: American Journal of Science, v. 301, no. 6, p. 513-556.

White, R. J., Dunbar, N., Spinelli, G., and Mozley, P., Submitted, Glass Alteration and Cementation Offshore Japan: GSA Bulletin.

Yuasa, M., and Nohara, M., 1992, Petrographic and geochemical along-arc variations of volcanic rocks on the volcanic front of the Izu-Ogasawara (Bonin) Arc: Bulletin of the Geological Survey of Japan, v. 43 no. 7, p. 421-456.Berger, G., Schott, J., and Loubet, M., 1987, FUNDAMENTAL PROCESSES CONTROLLING THE 1ST STAGE OF ALTERATION OF A BASALT GLASS BY SEAWATER - AN EXPERIMENTAL-STUDY BETWEEN 200-DEGREES-C AND 320-DEGREES-C: Earth and Planetary Science Letters, v. 84, no. 4, p. 431-445.

Brocher, T. M., Fuis, G. S., Fisher, M. A., Plafker, G., Moses, M. J., Taber, J. J., and Christensen, N. I., 1994, MAPPING THE MEGATHRUST BENEATH THE NORTHERN GULF OF ALASKA USING WIDE-ANGLE SEISMIC DATA: Journal of Geophysical Research-Solid Earth, v. 99, no. B6, p. 11663-11685.

Chamot-rooke, N., Renard, V., and Le Pichon, X., 1987, MAGNETIC-ANOMALIES IN THE SHIKOKU BASIN - A NEW INTERPRETATION: Earth and Planetary Science Letters, v. 83, no. 1-4, p. 214-228.

Clough, G. W., Sitar, N., Bachus, R. C., and Rad, N. S., 1981, CEMENTED SANDS UNDER STATIC LOADING: Journal of the Geotechnical Engineering Division-Asce, v. 107, no. 6, p. 799-817.

Crovisier, J. L., Thomassin, J. H., Juteau, T., Eberhart, J. P., Touray, J. C., and Baillif, P., 1983, EXPERIMENTAL SEAWATER BASALTIC GLASS INTERACTION AT 50-DEGREES-C - STUDY OF EARLY DEVELOPED PHASES BY ELECTRON-MICROSCOPY AND X-RAY PHOTOELECTRON SPECTROMETRY: Geochimica Et Cosmochimica Acta, v. 47, no. 3, p. 377-387.

Fox, P. J., 1996, Backarc basins. Tectonics and magmatism - Taylor,B: Science, v. 272, no. 5258, p. 43-43.

Hajash, A., and Chandler, G. W., 1981, An experimental investigation of high-temperature interactions between seawater and rhyolite, andesite, basalt and peridotite Contributions to Minerology and Petrology, v. 78, no. 3, p. 240-254.

Huang, T. C., 1980, A volcanic sedimentation model: Implications of processes and responses of deep-sea ashes: Marine Geology, v. 38, no. 1-3, p. 103-122.

Karig, D., 1993, Reconsolidation tests and sonic velocity measurements of clay-rich sediments from the Nankai Trough, Proceedings of the Ocean Drilling Program.

Larsen, G., 1983, EARLY DIAGENESIS - A THEORETICAL APPROACH - BERNER,RA: Earth-Science Reviews, v. 19, no. 2, p. 174-175.

Okino, K., Shimakawa, Y., and Nagaoka, S., 1994, EVOLUTION OF THE SHIKOKU BASIN: Journal of Geomagnetism and Geoelectricity, v. 46, no. 6, p. 463-479.

Reed, S. J. B., 1996, Electron Microprobe and Scanning Electron Microscopy in Geology, Cambridge University Press.

Saidi, F., Bernabe, Y., and Reuschle, T., 2003, The mechanical behaviour of synthetic, poorly consolidated granular rock under uniaxial compression: Tectonophysics, v. 370, no. 1-4, p. 105-120.

Schiffman, P., Watters, R. J., Thompson, N., and Walton, A. W., 2006, Hyaloclastites and the slope stability of Hawaiian Volcanoes: Insights from the Hawaiian Scientific Drilling Project's 3-km drill core, p. 217-228.

Schnaid, F., Prietto, P. D. M., and Consoli, N. C., 2001, Characterization of cemented sand in triaxial compression: Journal of Geotechnical and Geoenvironmental Engineering, v. 127, no. 10, p. 857-868.

Spinelli, G. A., Mozley, P. S., Tobin, H. J., Underwood, M. B., Hoffman, N. W., and Bellew, G. M., 2007, Diagenesis, sediment strength, and pore collapse in sediment approaching the Nankai Trough subduction zone: Geological Society of America Bulletin, v. 119, no. 3-4, p. 377-390.

Zhou, W. M., Peacor, D. R., Alt, J. C., Van der Voo, R., and Kao, L. S., 2001, TEM study of the alteration of interstitial glass in MORB by inorganic processes, p. 365-376.

APPENDIX

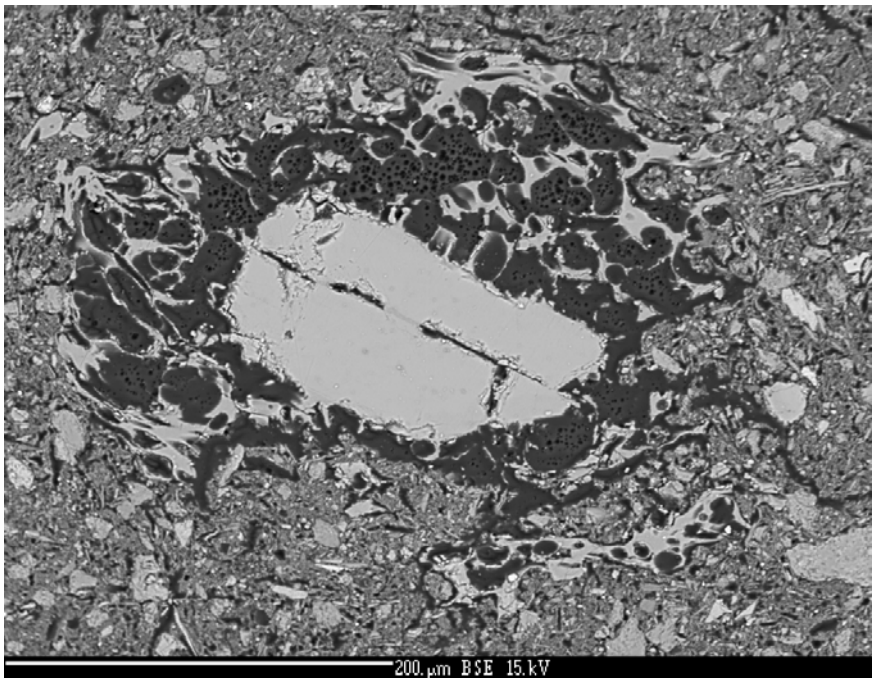

Figure A1: Sample 297-12 (249 mbsf) vesiculated glass surrounding feldspar grain.

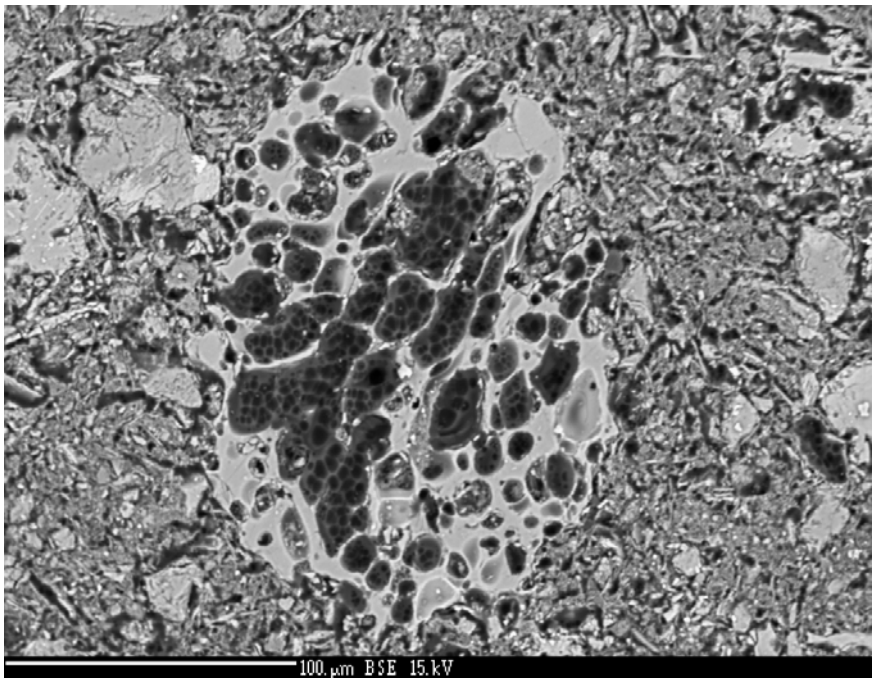

Figure A2: Sample 297-12 (249 mbsf) vesiculated glass.

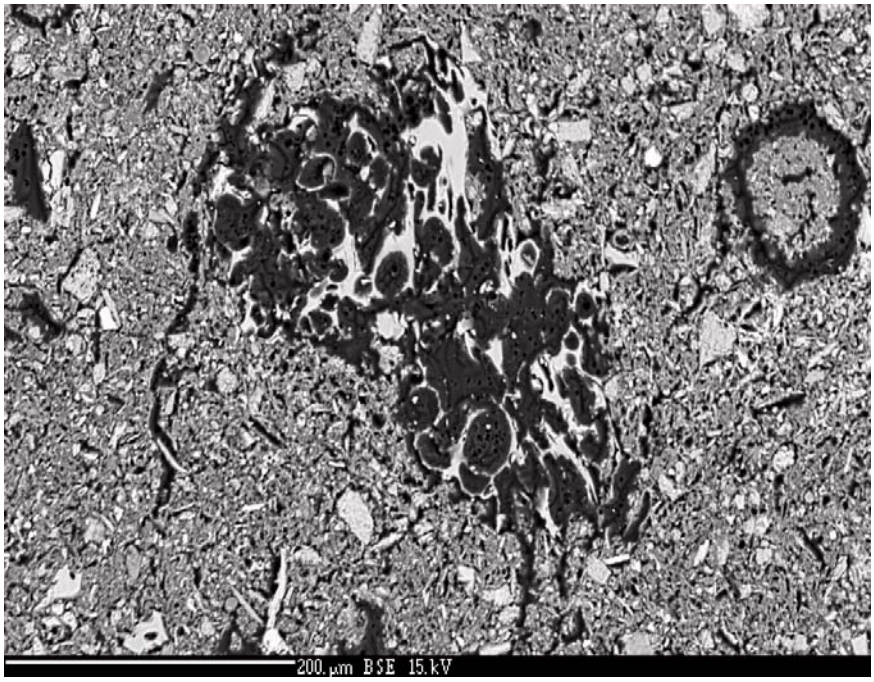

Figure A3: Sample 297-12 (249 mbsf) highly dissolved vesiculated glass.

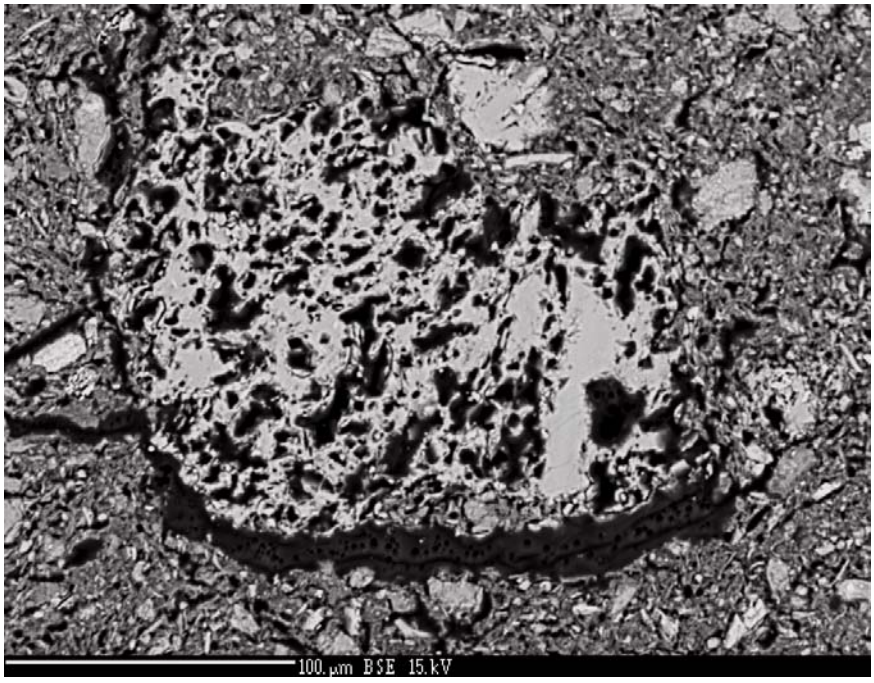

Figure A4: Sample 297-12 (249 mbsf) highly dissolved vesiculated glass.

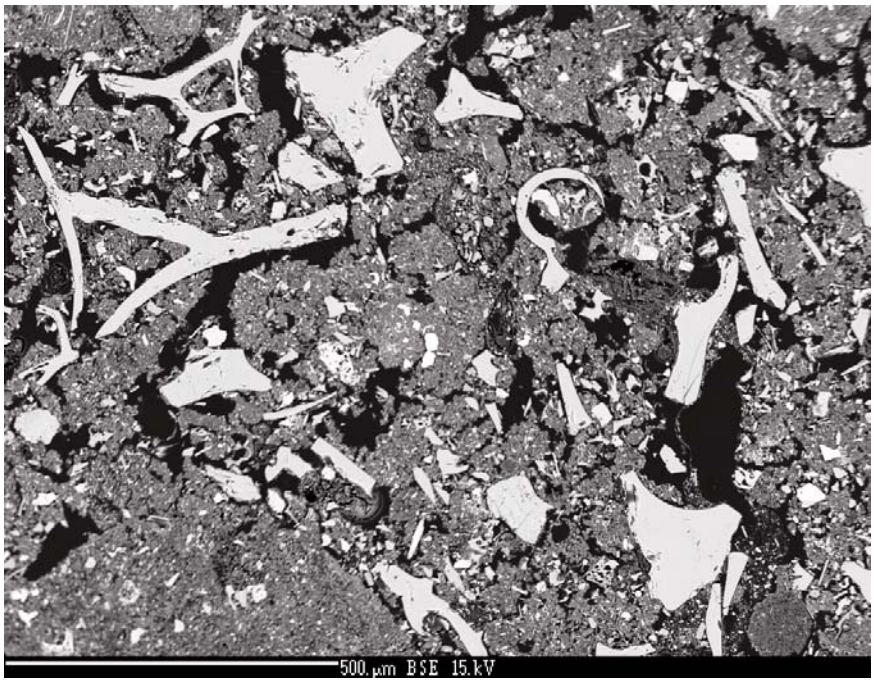

Figure A5: Sample 442-28 (258 mbsf) large glass triple junctions and small glass fragments in clay matrix.

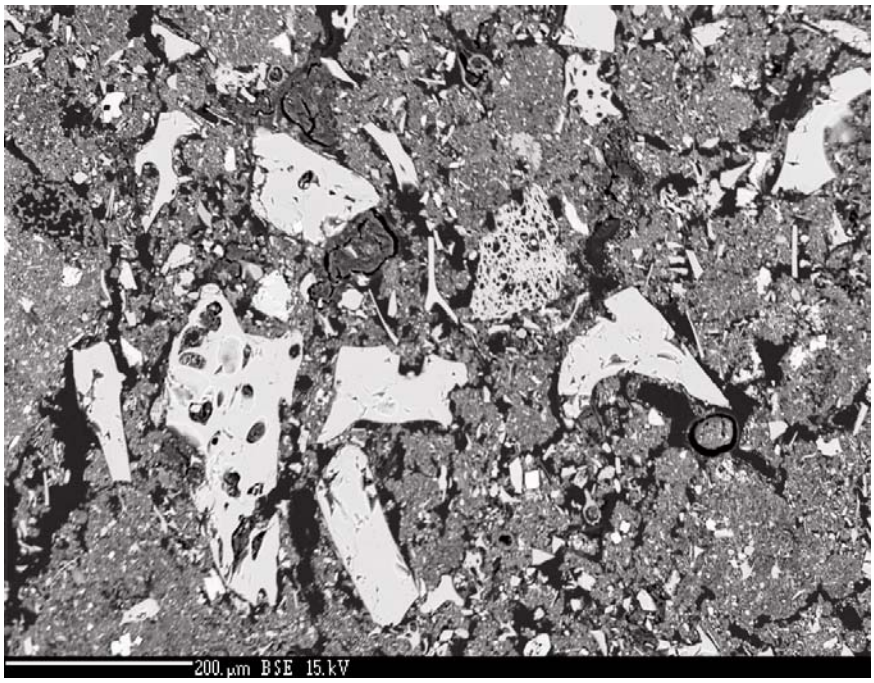

Figure A6: Sample 442-28 (258 mbsf) large blocky vesicular glass pieces and small glass fragments in clay matrix.

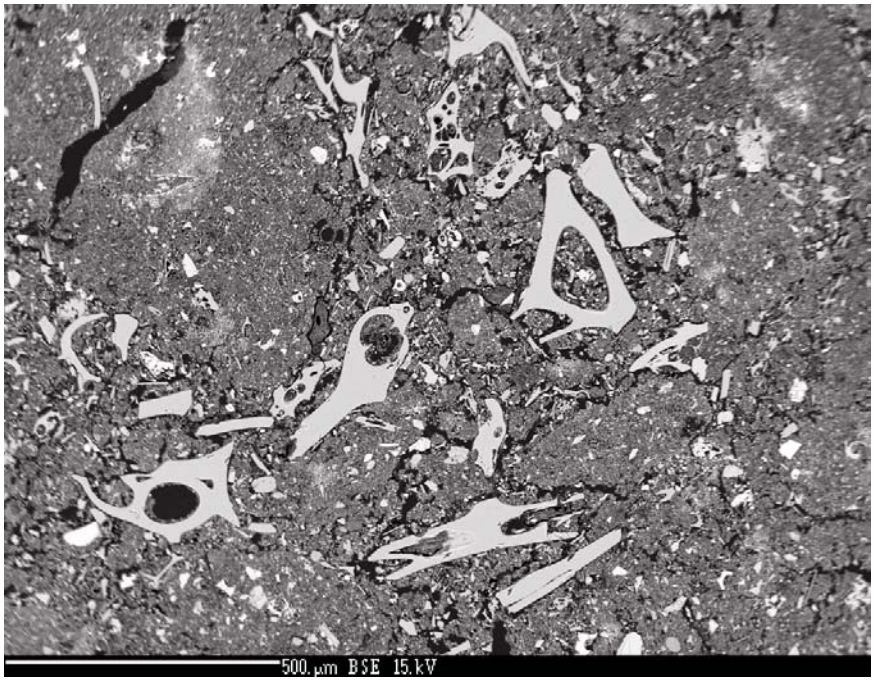

Figure A7: Sample 442-28 (258 mbsf) large glass bubble walls and small vesiculated glass in clay matrix.

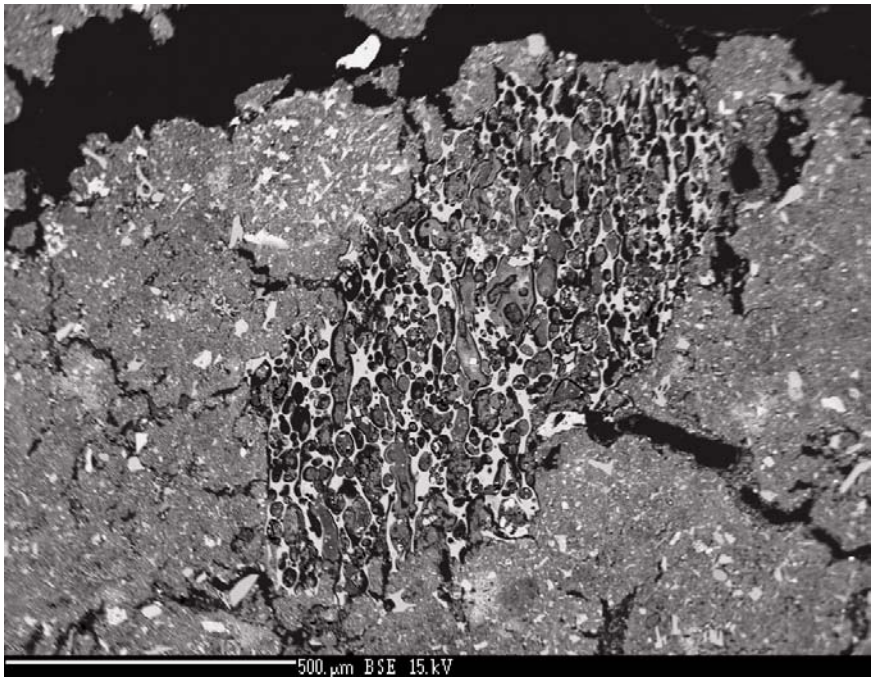

Figure A8: Sample 442-28 (258 mbsf) large vesiculated glass in clay matrix.

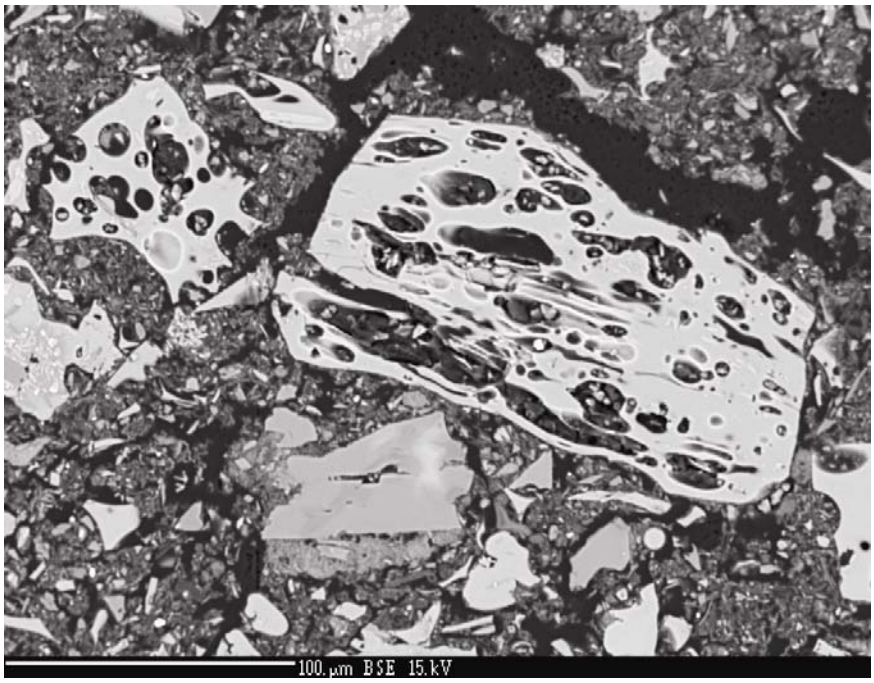

Figure A9: Sample 443-30 (275 mbsf) vesiculated glass, small glass pieces and detrital quartz in clay matrix.

Figure A10: Sample 443-30 (275 mbsf) large glass bubble wall in clay matrix.

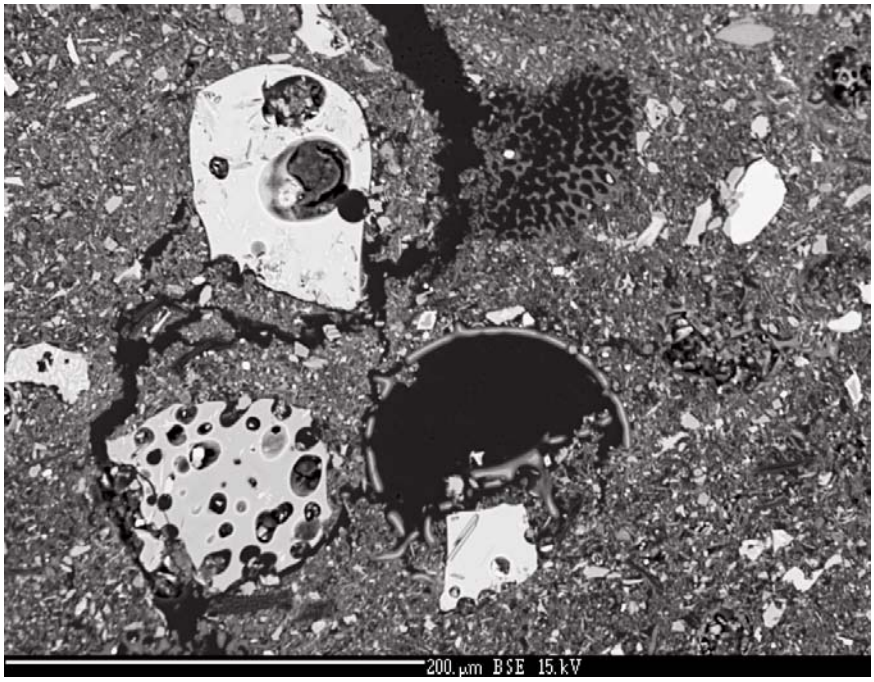

Figure A11: Sample 443-30 (275 mbsf) large blocky vesiculated glass, with carboniferous and siliceous microfossils in clay matrix.

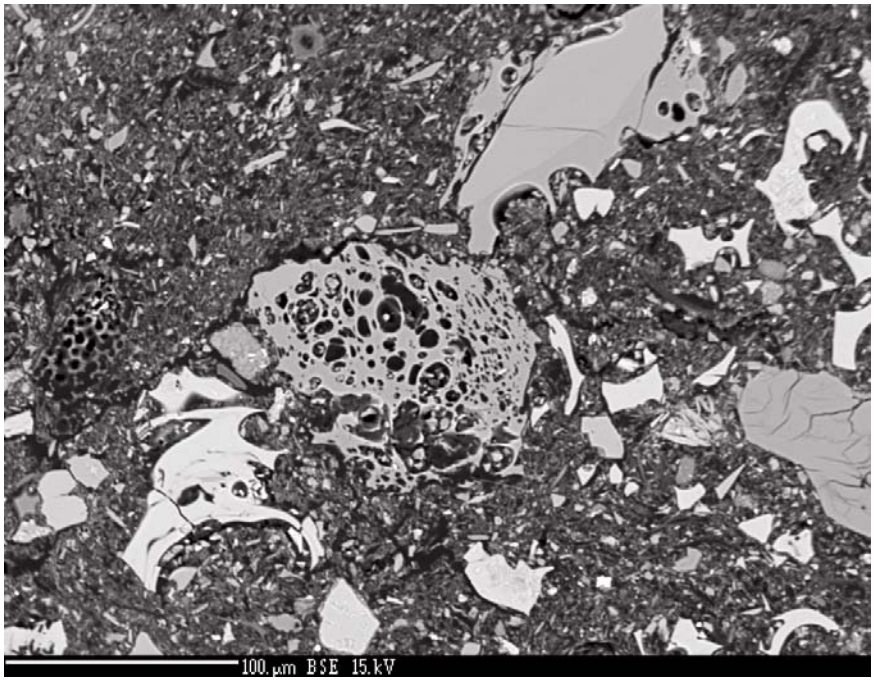

Figure A12: Sample 443-30 (275 mbsf) vesiculated glass, small glass pieces and detrital quartz in clay matrix.

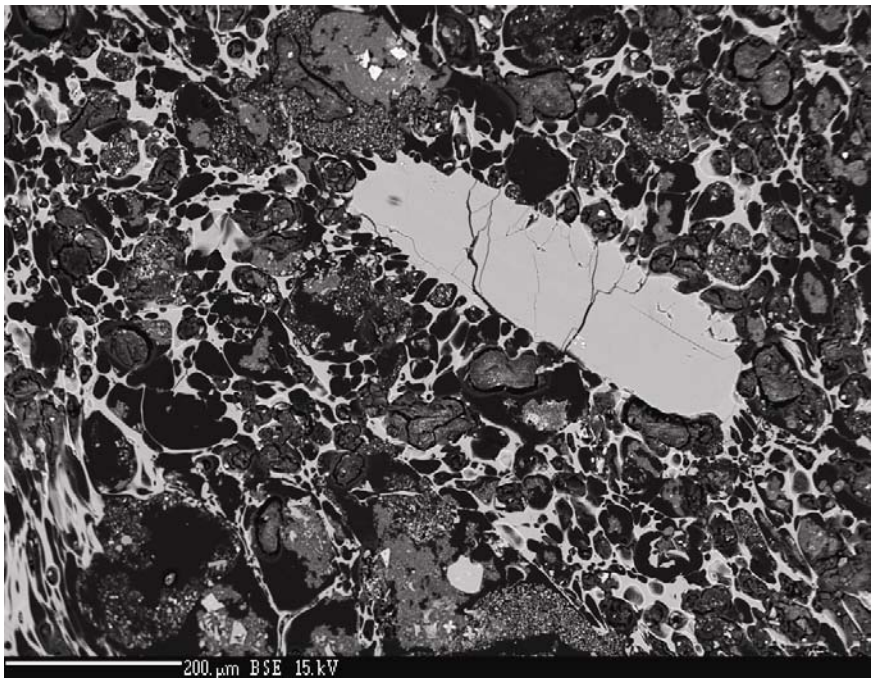

Figure A13: Sample 443-34 (317 mbsf) large vesiculated glass surrounding feldspar grain, minor amount of clay.

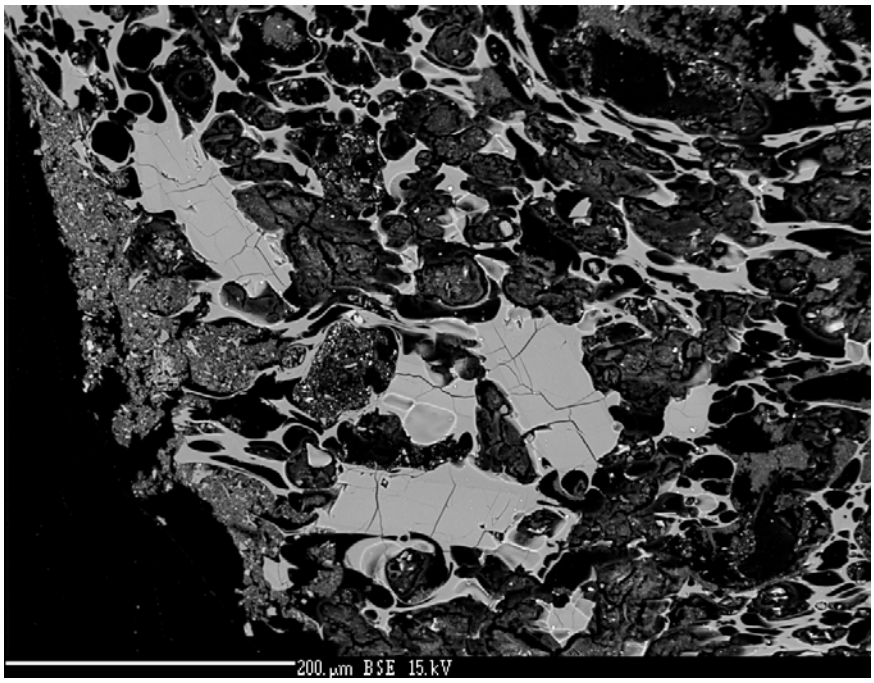

Figure A14: Sample 443-34 (317 mbsf) large vesiculated glass surrounding multiple feldspar grains, minor amount of clay.

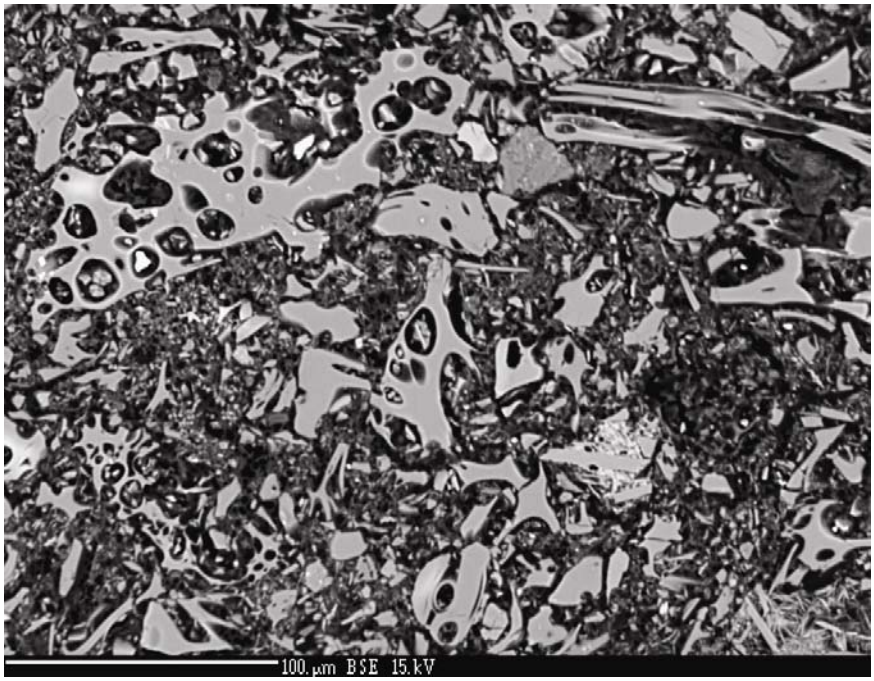

Figure A15: Sample 443-34 (317 mbsf) vesiculated glass, small glass pieces and detrital quartz in clay matrix.

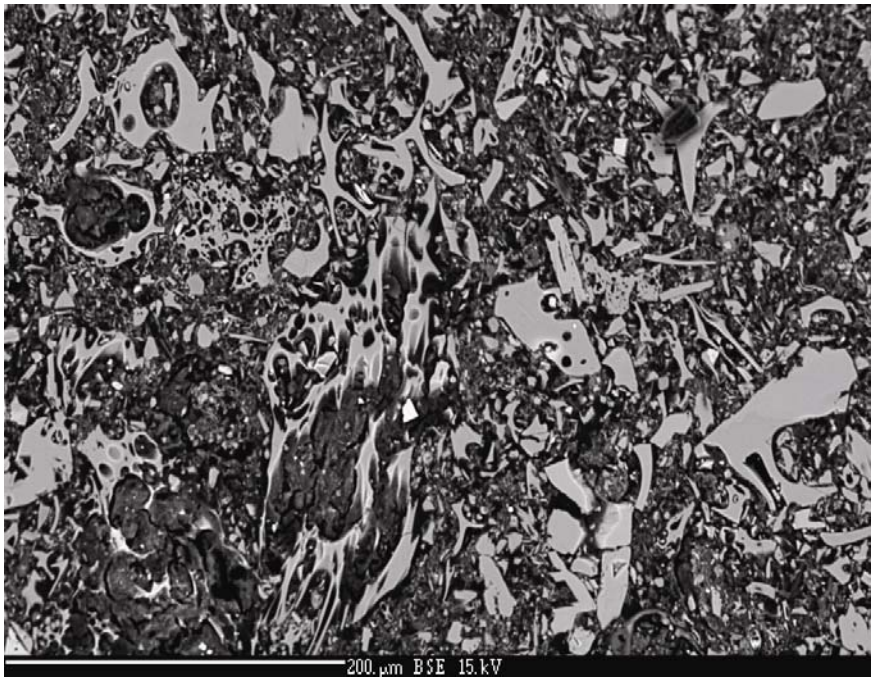

Figure A16: Sample 443-34 (317 mbsf) vesiculated glass, small glass pieces and detrital quartz in clay matrix.

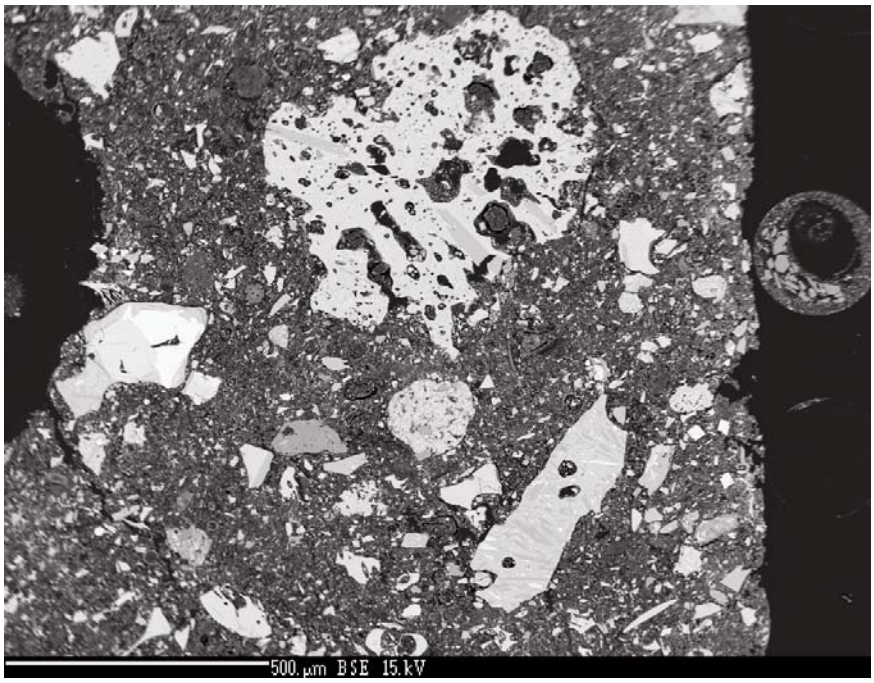

Figure A17: Sample 444-13 (198 mbsf) large vesiculated glass, small glass pieces and detrital quartz in clay matrix.

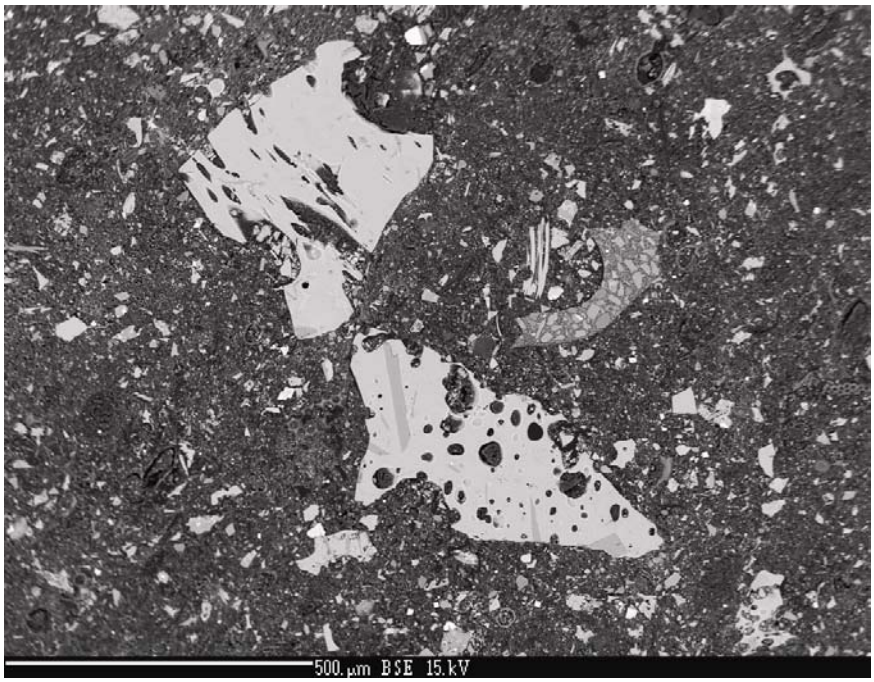

Figure A18: Sample 444-13 (198 mbsf) large blocky vesiculated glass and small glass pieces in clay matrix.

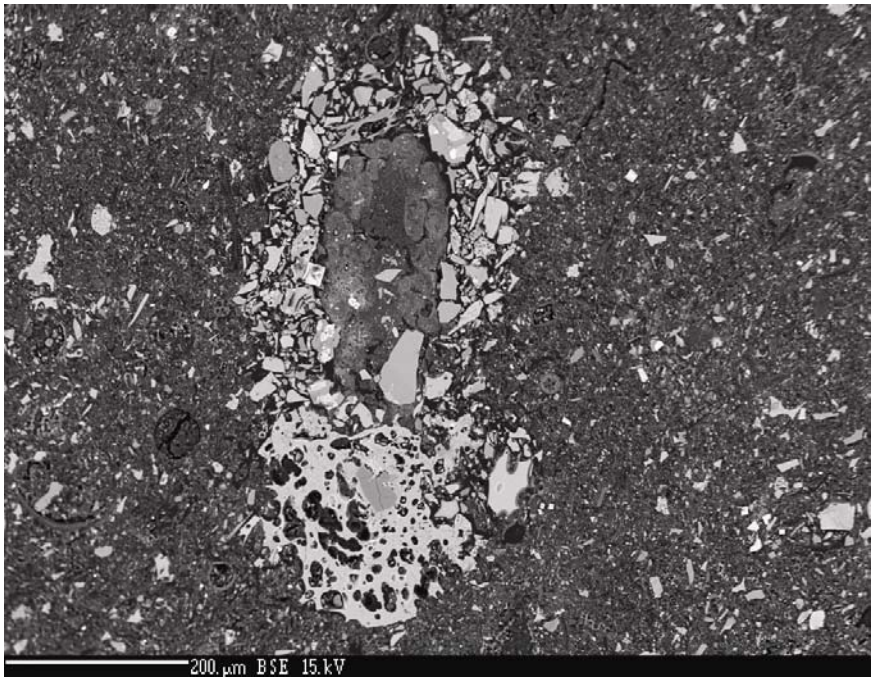

Figure A19: Sample 444-13 (198 mbsf) large blocky vesiculated glass, small glass pieces and detrital quarts emplaced through bioturbation in clay matrix.

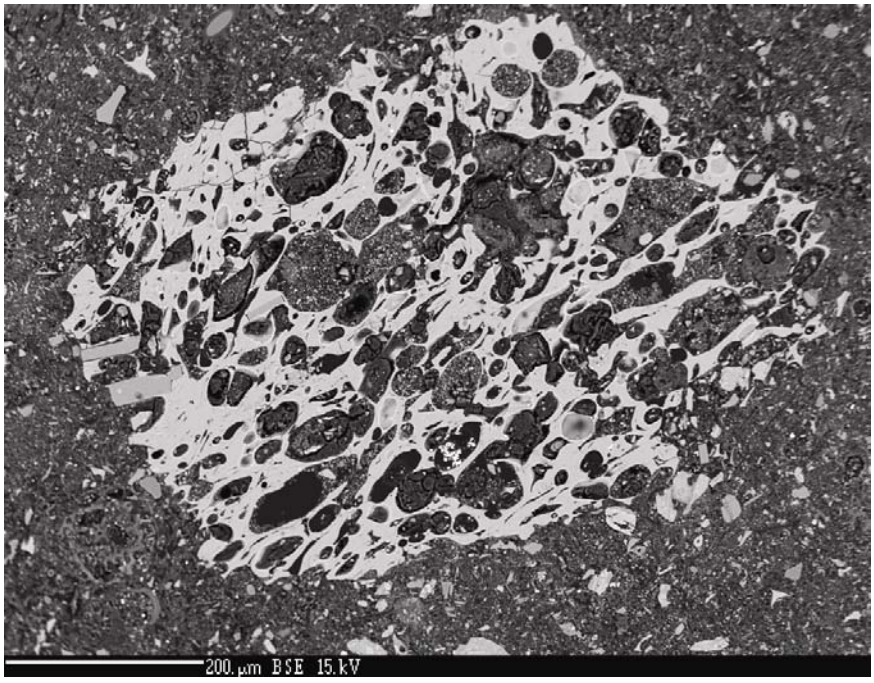

Figure A20: Sample 444-13 (198 mbsf) large vesiculated glass and small glass pieces in clay matrix.

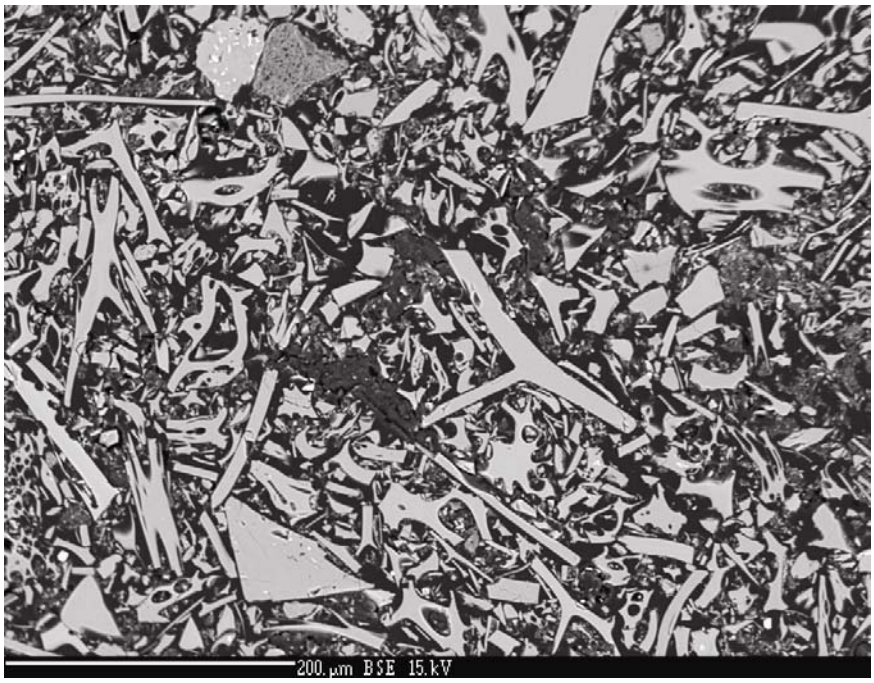

Figure A21: Sample 444-16 (226 mbsf) glass wall triple junctions and small vesiculated glass pieces with minor amount of clay.

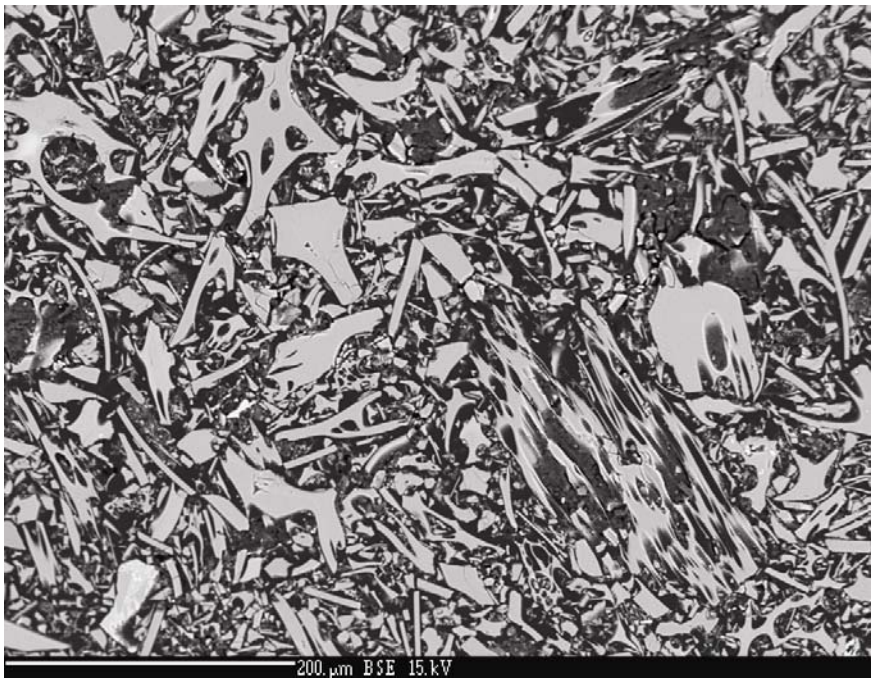

Figure A22: Sample 444-16 (226 mbsf) glass wall triple junctions and vesiculated glass pieces with minor amount of clay.

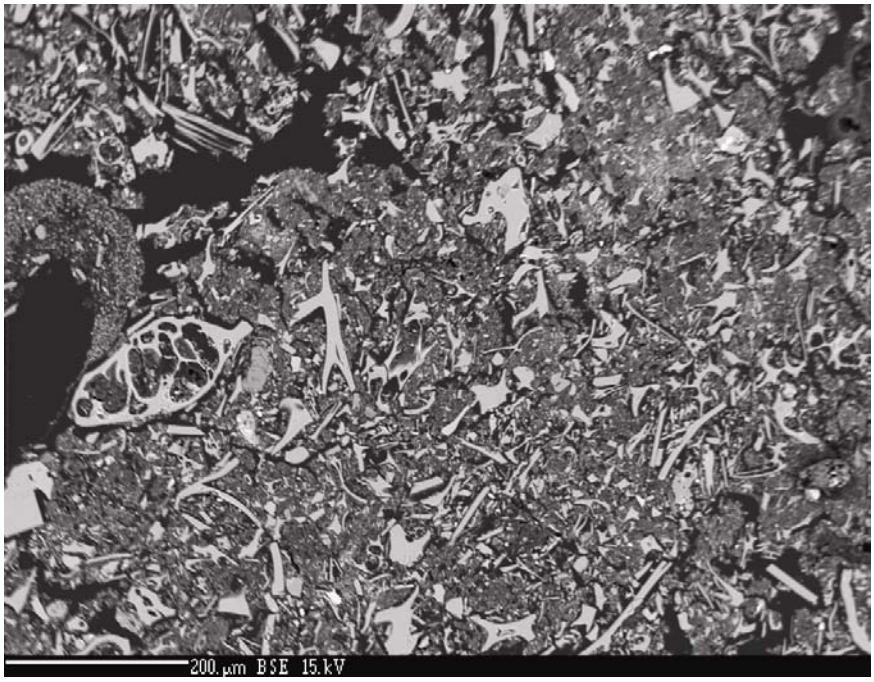

Figure A23: Sample 444-16 (226 mbsf) fine grained glass wall triple junctions and vesiculated glass pieces in clay matrix.

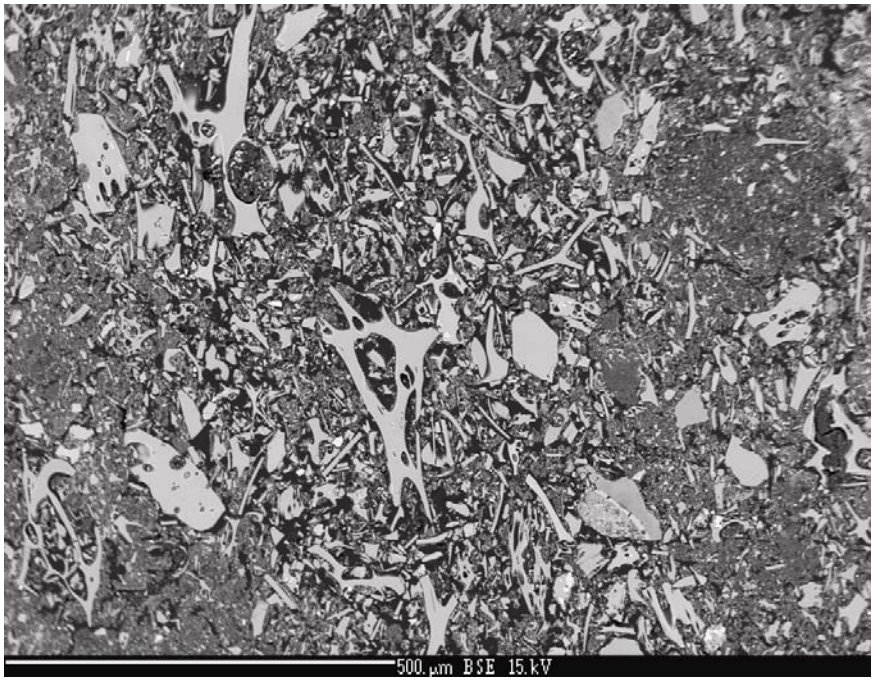

Figure A24: Sample 444-16 (226 mbsf) glass wall triple junctions and vesiculated glass pieces in clay matrix.